Neurobiology of Disease 188 (2023) 106341

Contents lists available at ScienceDirect

Neurobiology of Disease

journal homepage: www.elsevier.com/locate/ynbdi

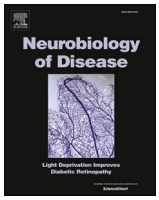

Boolean analysis shows a high proportion of dopamine D_2 receptors interacting with adenosine A_{2A} receptors in striatal medium spiny neurons of mouse and non-human primate models of Parkinson's disease

Rafael Rivas-Santisteban [a,b,*], Alberto José Rico [b,c], Ana Muñoz [b,d], Ana I. Rodríguez-Pérez [b,d], Irene Reyes-Resina [b,e], Gemma Navarro [b,e,f], José Luis Labandeira-García [b,d], José Luis Lanciego [b,c], Rafael Franco [b,g,h,*]

[a] Laboratory of Computational Medicine, Biostatistics Unit, Faculty of Medicine, Autonomous University of Barcelona, Campus Bellaterra, 08193 Barcelona. Spain
[b] Network Center for Biomedical Research in Neurodegenerative Diseases, CiberNed, Spanish National Health Institute Carlos iii, Av. Monforte de Lemos, 3-5, 28029 Madrid, Spain
[c] CNS Gene Therapy Department, Center for Applied Medical Research (CIMA, IdiSNA), University of Navarra, Pamplona, Spain
[d] Cellular and Molecular Neurobiology of Parkinson's Disease, Research Center for Molecular Medicine and Chronic Diseases (CIMUS), IDIS, University of Santiago de Compostela, Santiago de Compostela, Spain
[e] Department of Biochemistry and Physiology, School of Pharmacy and Food Sciences, Universitat de Barcelona, 08028 Barcelona, Spain
[f] Institute of Neuroscience of the University of Barcelona, Universitat de Barcelona, 08028 Barcelona, Spain
[g] Molecular Neurobiology laboratory, Dept. Biochemistry and Molecular Biomedicine, Facultat de Biologia, Universitat de Barcelona, 08028 Barcelona, Spain
[h] School of Chemistry, Universitat de Barcelona. Barcelona, Spain

ARTICLE INFO

Keywords:
GPCRs in heteromers
Direct pathway
Indirect pathway
Levodopa
Receptor-receptor interaction
Dyskinesia
MPTP

ABSTRACT

The antagonistic effect of adenosine on dopaminergic transmission in the basal ganglia indirect motor control pathway is mediated by dopamine D_2 (D_2R) and adenosine A_{2A} ($A_{2A}R$) receptors co-expressed on medium spiny striatal neurons. The pathway is unbalanced in Parkinson's disease (PD) and an $A_{2A}R$ blocker has been approved for use with levodopa in the therapy of the disease. However, it is not known whether the therapy is acting on individually expressed receptors or in receptors forming A_{2A}-D_2 receptor heteromers, whose functionality is unique. For two proteins prone to interact, a very recently developed technique, MolBoolean, allows to determine the number of proteins that are either non-interacting or interacting. After checking the feasibility of the technique and reliability of data in transfected cells and in striatal primary neurons, the Boolean analysis of receptors in the striatum of rats and monkeys showed a high percentage of D_2 receptors interacting with the adenosine receptor, while, on the contrary, a significant proportion of A_{2A} receptors do not interact with dopamine receptors. The number of interacting receptors increased when rats and monkeys were lesioned to become a PD model. The use of a tracer of the indirect pathway in monkeys confirmed that the data was restricted to the population of striatal neurons projecting to the GPe. The results are not only relevant for being the first study quantifying individual versus interacting G protein-coupled receptors, but also for showing that the D_2R in these specific neurons, in both control and PD animals, is under the control of the $A_{2A}R$. The tight adenosine/dopamine receptor coupling suggest benefits of early antiparkinsonian treatment with adenosine receptor blockers.

1. Introduction

Striatum shows the highest expression of the adenosine A_{2A} receptor ($A_{2A}R$). The receptor exerts a variety of functions in both glia and neurons. Decades ago, it was demonstrated that adenosine, via the $A_{2A}R$, antagonizes dopaminergic neurotransmission mediated by the D_2R. The

Abbreviations: $A_{2A}R$, adenosine A_{2A} receptor; D_2R, dopamine D_2 receptor; A_{2A}-D_2Hets, A_{2A}-D_2 receptors heteromers; GPCR, G protein-couple receptor; PD, Parkinson's disease; RCPs, Rolling Circle replication Products; GRiH, GPCRs in heteromers.

* Corresponding author at: Network Center for Biomedical Research in Neurodegenerative Diseases, CiberNed, Spanish National Health Institute Carlos iii, Av. Monforte de Lemos, 3-5, 28029 Madrid, Spain.

E-mail addresses: rrivasbioq@gmail.com (R. Rivas-Santisteban), rfranco123@gmail.com, rfranco@ub.edu (R. Franco).

https://doi.org/10.1016/j.nbd.2023.106341
Received 7 September 2023; Received in revised form 16 October 2023; Accepted 30 October 2023
Available online 31 October 2023

anatomical basis of this fact is the expression of $A_{2A}R$ in γ-amino butyric acid (GABA) medium spiny neurons of the so-called indirect pathway (Parent and Hazrati, 1993), which are characterized by the expression of the dopamine D_2 receptor (D_2R). The antagonism was first noted at the functional level until a direct interaction between the two receptors was demonstrated (Franco et al., 2000; Hillion et al., 2002).

$A_{2A}R$ and D_2R are G protein-coupled receptors (GPCRs) that couple to, respectively, $G_{s/olf}$ and G_i proteins (Alexander et al., 2021). Heteromers formed by the interaction of two GPCRs lead to macromolecular complexes whose functionality is different from that of the partner receptors when individually expressed. Receptor heteromerization leads to particular properties/imprints such as differential functional selectivity, shift of G protein coupling and inter-receptor allosteric modulations occurring both in the presence or absence of receptor ligands (Feltmann et al., 2018; Huang et al., 2013). GPCRs in heteromers (GRiH) arise as novel targets for drug development. The receptors constituting the A_{2A}-D_2 receptor heteromer (A_{2A}-D_2Het), which is expressed in striatal neurons, are considered a target of Parkinson's disease (PD). Previous studies have shown in animal models of PD that the A_{2A}-D_2Het is disrupted upon treatment with levodopa, which is the main therapy used to manage the disease. Electrophysiological studies have detected abnormalities in parkinsonian animals treated with levodopa, which could be related with a variation in the proportion of $A_{2A}R$-containing heteromers (Antonelli et al., 2006; Beggiato et al., 2016). The evidence on the participation of the $A_{2A}R$ in controlling dopaminergic transmission and preclinical assays testing $A_{2A}R$ antagonists in PD animal models led to clinical trials to test efficacy of such compounds in the therapy of PD (Chen et al., 2001; Morelli et al., 2007; Schwarzschild et al., 2006, 2002). Finally, a first-in-class $A_{2A}R$ antagonist, istradefylline, was approved in Japan and the US for coadjuvant therapy of the disease (Jenner, 2014; Jenner et al., 2021; Saki et al., 2013). Noteworthy is the differential sensitivity of the $A_{2A}R$ to antagonists (Orru et al., 2011) and of dopamine receptors to agonists (Verma et al., 2010) depending on the heteromeric context. In fact, antagonists defined as selective using individually expressed $A_{2A}Rs$ can be stratified into different subtypes depending on whether the $A_{2A}R$ are forming heteromers with dopamine D_2 receptors in the postsynaptic membrane or with other GPCRs in the pre-synaptic membrane (Orru et al., 2011).

The adenosine-dopamine antagonistic interactions in the motor control circuits of the central nervous system have been known for decades. Interestingly, they are segregated in terms of basal ganglia circuits and of receptor types. There is an antagonism on the G_s-coupled D_1 receptor expressed in direct pathway neurons mediated by the G_i-coupled adenosine A_1 receptor, while there is an antagonism on the G_i-coupled D_2 receptor expressed in neurons of the indirect pathway mediated by the G_s-coupled adenosine A_{2A} receptor. At first it was thought that the functional interaction consisted of a counterbalance at the level of cAMP, the second messenger. In fact, activation of a G_i-coupled receptor that is linked to inhibition of adenylate cyclase would be counteracted by a G_s-coupled receptor that is linked to the activation of the cAMP-producing enzyme. The discovery of adenosine/dopamine receptor interactions prompted the hypothesis of further control mechanisms mediated by the unique properties of the A_{2A}-D_2Het, whose functionality is different from what might be expected from the signaling of individual D_2 and A_{2A} receptors (Ferre et al., 1993; Ferré et al., 2001; Fuxe et al., 2007; Strömberg et al., 2000). However, the robust expression of $A_{2A}Rs$ in striatum, which is higher than that of D_2Rs, and some actions mediated by the $A_{2A}R$ occurring in the absence of dopamine suggest that the role of the $A_{2A}R$ in motor control is not circumscribed to the functionality of the A_{2A}-D_2Het (see (Mori, 2020) for review). In this scenario, it is crucial to evaluate the proportion of $A_{2A}R$ and/or D_2R that are forming heteromers, something that has proven difficult to achieve due to lack of adequate technology.

The mechanisms underlying heteromer formation and cell surface targeting, and of internalization to be degraded in lysosomes or to be recycled back to the cell surface are not known. Challenging is also the confirmation of suspected plastic changes allowing for a given receptor to leave a partner and establish another interaction with a different one. A recently described novel technique has made possible for two interacting proteins to identify, in a given sample, the proportion of monomers/homomers and the proportion of heteromers (Raykova et al., 2022). The aim of this study was to assess, for the first time, the proportion of individual $A_{2A}R$, of individual D_2R and of $A_{2A}R$-D_2R heteromers present in primary cultures of striatal neurons. More importantly, we also aimed to assess the proportion of "free" and "complexed" A_{2A} and D_2 receptors in striatal sections of a rodent 6-OHDA PD model, before and after levodopa administration, and of a primate MPTP model of PD, with and without dyskinesias. In monkeys, quantification of the number of monomers versus heteromers was specifically addressed in striatal neurons retrogradely labeled using biotinylated dextran amines (BDA). Assessing and comparing the ratio of individual receptors and A_{2A}-D_2 receptor complexes in these animal models provides critical information on the pathogenesis and therapy of PD.

2. Results

2.1. Boolean analysis of A_{2A} and D_2 receptor interactions in heterologous cells and in primary striatal neurons

"*MolBoolean*" is an imaging technique recently developed to quantitate, for a pair of interacting proteins, which is the proportion of monomers and dimers in cells and in tissues (Raykova et al., 2022). A scheme of the technique, whose details are provided in the Methods section, is presented in Fig. 1. First, we used a heterologous system, namely HEK-293 T cells expressing $A_{2A}R$ and D_2R, to compare the signal coming from individual $A_{2A}Rs$, from individual D_2Rs, and from A_{2A}-D_2Hets. The two primary antibodies are highly specific, one monoclonal (anti-$A_{2A}R$) and another polyclonal (anti-D_2R); they have been widely used and validated in different laboratories and using KO animals (Rosin et al., 1998; Trifilieff et al., 2011) and in Labome (https://www.labome.com/knockout-validated-antibodies/A2A-antibody-knockout-validation-Millipore-05-717.html; accessed on October 12, 2023). Specificity of the antibodies has been shown in several articles coming from different laboratories. The monoclonal anti-$A_{2A}R$ antibody is commercially available from several sources and it is the same that was developed an characterized in the laboratory of Joel Linden in 1998 (Rosin et al., 1998). We and others have used the monoclonal antibody to specifically label the $A_{2A}R$ in brain sections and/or the $A_{2A}R$ expressed in heterologous systems (Carriba et al., 2007; Orr et al., 2015). As an example, a 1:200 dilution has been used to label the $A_{2A}R$ in mouse cortex and striatum sections (Orr et al., 2015); in our tests, 1:250 dilution was used. The AB5084P (Merck) polyclonal anti-D_2R antibody is also specific as it has been demonstrated in different laboratories. Stojanovic et al., 2017, have specifically validated antibodies against dopamine receptors using receptor-deficient mice and AB5084P was considered as specific for labeling the D_2R (Stojanovic et al., 2017). The antibody was tested in HEK-293 T cells, untransfected and transfected using a cDNA coding for the human version of the D_2R. The results show that the label due to AB5084P was only detected in cells expressing the D_2R (Supplementary Fig. S1). In addition, the control consisting of lack of significant label in neurons of the direct pathway (see below) is a further proof of the high specificity of the primary antibodies used.

MolBoolean™ assay technical positive controls were performed in HEK-293 T cells coexpressing $A_{2A}R$ and D_2R. Negative controls included omitting either the anti-$A_{2A}R$ or the anti-D_2R primary antibodies and omitting probe A or probe B. These controls validated the specificity of the MolBoolean assay by demonstrating a lack of fluorescent signal when these components were omitted (Supplementary Fig. S2).

MolBoolean analysis was performed in cells cotransfected with plasmids coding for the human versions of the $A_{2A}R$ and of the D_2R. In this system that mildly overexpresses the two receptors, the technique identifies all three types of signals, namely those corresponding to

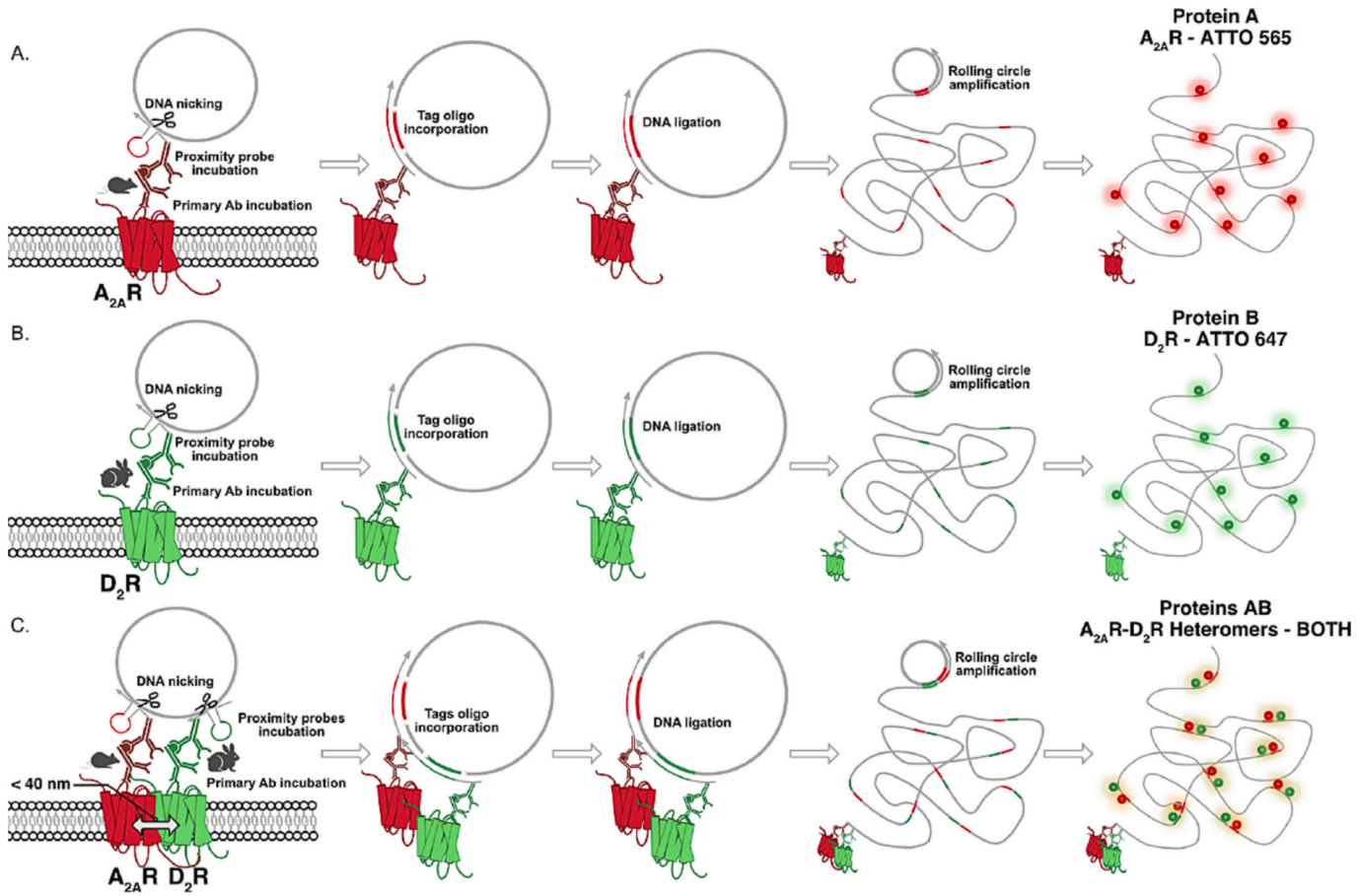

Fig. 1. Scheme of the MolBoolean™ method to detect individual and interacting A_{2A} and D_2 receptors. A_{2A}R and D_2R are targeted with, respectively, specific mouse and rabbit primary antibodies. After that, anti-mouse and anti-rabbit secondary antibodies conjugated with specific oligonucleotide probes were incubated with the samples. DNA oligonucleotides hybridized with a circular probe, forming double-stranded regions recognized by the nickase enzyme (depicted as a black scissor). Subsequently, oligomeric tags are incorporated into the circular probe and ligated. Through a process of rolling circle amplification, Rolling Circle replication Products (RCPs) are created. RCPs were detected using ATTO565 (A_{2A}R detection, A), ATTO647 (D_2R detection, B) and both (A_{2A}-D_2Het detection, C).

individual receptors, A_{2A} and D_2, and to the A_{2A}-D_2Het. A deconvolution process was performed on the images to facilitate subsequent processing and quantification of the receptor complexes (Fig. 2A). Magnification images in Fig. 2B show that it is possible to differentiate between red, green and yellow dots and, therefore, and ad hoc procedure was developed using the CellProfiler™ platform to perform quantification (see Methods). The data show that receptors were mainly found as heteromers (Fig. 2D).

After validation of the method and optimization of the quantification protocol, experiments were performed in rodent striatal neurons. Some of the primary neurons obtained from the striatum of mice were, as expected, expressing both receptors. The results clearly showed that in neurons expressing the two receptors, the amount of individually expressed D_2Rs was negligible. In contrast, the number of dots corresponding to the complexes formed by the two receptors stands out. Approximately half of the label corresponding to the A_{2A}R was found to be associated with that of the D_2R; the other half can come from the A_{2A}R, individually expressed or forming complexes with other proteins (Fig. 3).

2.2. *Boolean analysis of A_{2A} and D_2 receptor interactions in sections from a rat PD model*

Assays were performed in striatal sections of non-lesioned and lesioned animals with 6-OHDA treated or not with L-DOPA. Sections from 4 groups of animals were considered: non-lesioned (control), lesioned, lesioned treated with L-DOPA but not becoming dyskinetic and lesioned that upon L-DOPA treatment became dyskinetic. Only the ipsilateral hemisphere was considered. There were striatal cells expressing the two receptors in sections from all animal groups (Fig. 4). Quantification was performed using the control group as reference for normalization. Data showed a decrease in individually expressed A_{2A}Rs in lesioned animals and recovery upon L-DOPA administration (Fig. 4E). In contrast the population of individually expressed D_2Rs was decreased in lesioned animals and the L-DOPA treatment did not revert the decrease in non-dyskinetic animals. However, the level of D_2Rs was similar to non-lesioned (control) in samples from animals that became dyskinetic after L-DOPA administration (Fig. 4F). In agreement with these data, the level of A_{2A}R-D_2R complexes was significantly higher in sections from lesioned animals and from lesioned animals that did not become dyskinetic by L-DOPA administration; the level was like in controls in those animals that were rendered dyskinetic by L-DOPA treatment (Fig. 4G). Important information was obtained by quantifying the percentage of receptors, A_{2A}R or D_2R, that were forming complexes in the four conditions. The amount of D_2R in A_{2A}-D_2Hets was high in all conditions, even being nearly total (100%) in the case of lesioned animals treated with L-DOPA that did not become dyskinetic; around 80% in samples from dyskinetic animals (Fig. 4I). In sharp contrast, only the 13% the A_{2A}R expressed in striatal cells was forming complexes. The percentage of A_{2A}Rs in A_{2A}-D_2Hets significantly increased to approximately 42% in lesioned animals; the increase was small and/or insignificant in samples from lesioned animals treated with L-DOPA (Fig. 4H).

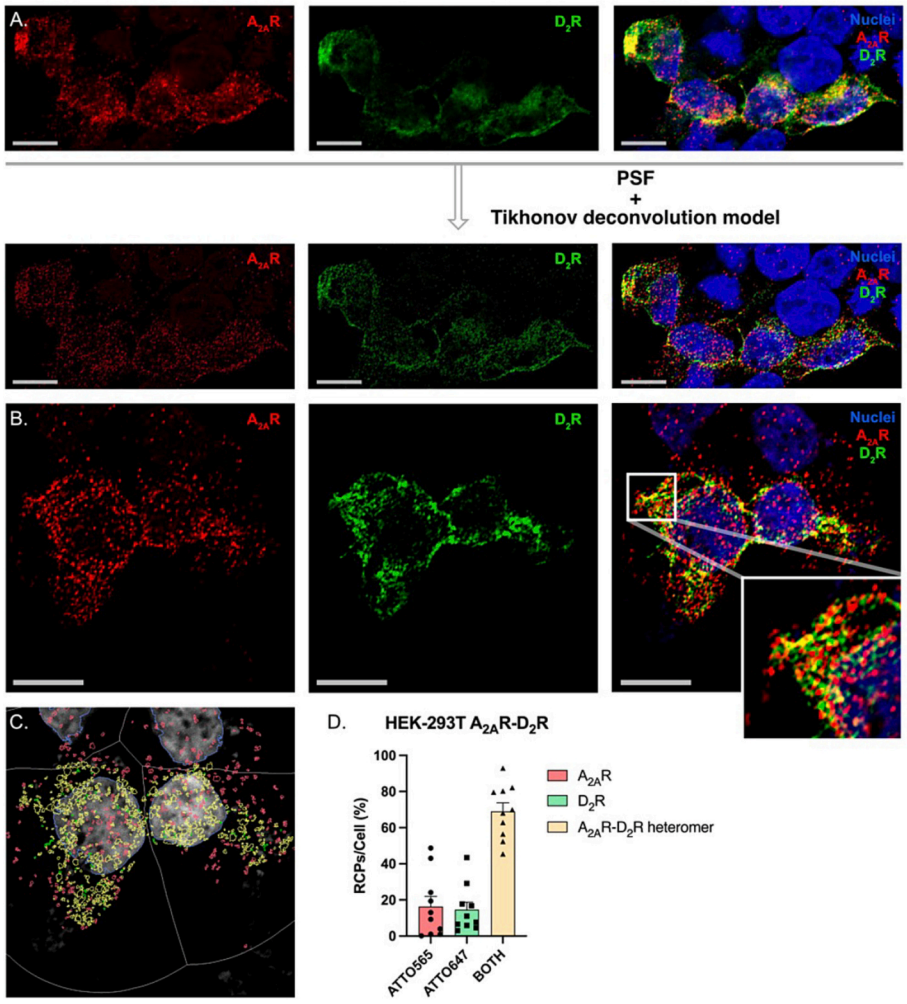

Fig. 2. MolBoolean analysis of $A_{2A}R$ and D_2R expression in HEK-293 T transfected cells. (A) Confocal images were deconvolved using the point spread function (PSF) and applying Tikhonov deconvolution model. Scale bar = 10 μm. (B) Assays were performed in HEK-293 T cells coexpressing A_{2A} and D_2 receptors. $A_{2A}R$ labeling is in red, D_2R labeling is in green, and labeling of complexes is in yellow. Hoechst staining of nuclei is shown in blue. Scale bar = 10 μm. (C) Using a specifically designed CellProfiler™ pipeline, quantification and analysis of the RCPs at the individual cell level were performed. (D) Quantification of RCPs per cell is expressed as a percentage of the total RCPs (the sum of red, green, and yellow dots). Values in the bar graph are the mean ± S.E.M. of 5 different experiments performed in triplicates: 16.4 ± 5.5 (red; $A_{2A}R$), 14.6 ± 4.15 (green; D_2R) and 69.0 ± 4.7 (yellow; A_{2A}-D_2Het). (For interpretation of the references to colour in this figure legend, the reader is referred to the web version of this article).

2.3. Assessing the amount of A_{2A}Rs and D_2Rs in heteromers in sections from the Macaca fascicularis PD model

2.3.1. Direct pathway

The 1-methyl-*4-phenyl-1,2,3,6*-tetrahydropyridine (MPTP)-based *Macaca fascicularis* PD model is considered the closest to human disease. Assays were performed in striatal sections of non-lesioned primates, of MPTP lesioned animals and of MPTP lesioned animals rendered dyskinetic upon chronic L-DOPA administration. In addition, GABAergic neurons projecting through the direct and indirect pathway were retrogradely labeled upon the delivery of the retrograde tracer, biotinylated dextran amine (BDA), into either the internal or external divisions of the globus pallidus (GPi and GPe, respectively) (Fig. 5A). Unlike the experiments carried out in the rat model, in which all cells expressing receptors were quantified, in the monkey model only the BDA-labeled neurons were considered.

Images in Fig. 5 B-G show the label corresponding to individual receptors and to receptor complexes in medium spiny neurons (MSNs) of the direct pathway of i) non-lesioned animals, ii) lesioned animals and iii) lesioned animals that became dyskinetic upon L-DOPA treatment. The level of both individual receptors and receptor complexes (total RCPs) was very low in striatal direct pathway and may serve as a control for the results found in the striatal indirect pathway. In fact, the amount of A_{2A} and D_2 receptors in complexes in MSNs of the direct pathway is negligible compared to that in neurons of the indirect pathway. The amount of RCPs in cells of the indirect pathway increased significantly in samples from lesioned animals although the increase was much higher in dyskinetic animals (Fig. 5 H). When comparing the amount of RCPs in cells of the indirect versus cells of the direct pathways the results were similar in control, lesioned and dyskinetic groups (Fig. 5 I—K).

2.3.2. Indirect pathway

Expression of A_{2A}-D_2 receptor complexes was notable in the neurons labeled with BDA and corresponding to the indirect pathway of control animals (Fig. 6). Whereas the D_2R was mainly found in complexes, less than half of the $A_{2A}R$ in those BDA-labeled neurons was forming complexes with the D_2R. The label corresponding to complexes in striatal neurons of the indirect pathway was significantly higher in both lesioned and dyskinetic animals in comparison with non-lesioned animals (Fig. 6 I). Non-interacting A_{2A}Rs and non-interacting D_2Rs decreased in striatal neurons of the indirect pathway of lesioned monkeys (Fig. 6 G-H). The percentage of $A_{2A}R$ in heteromers in neurons also

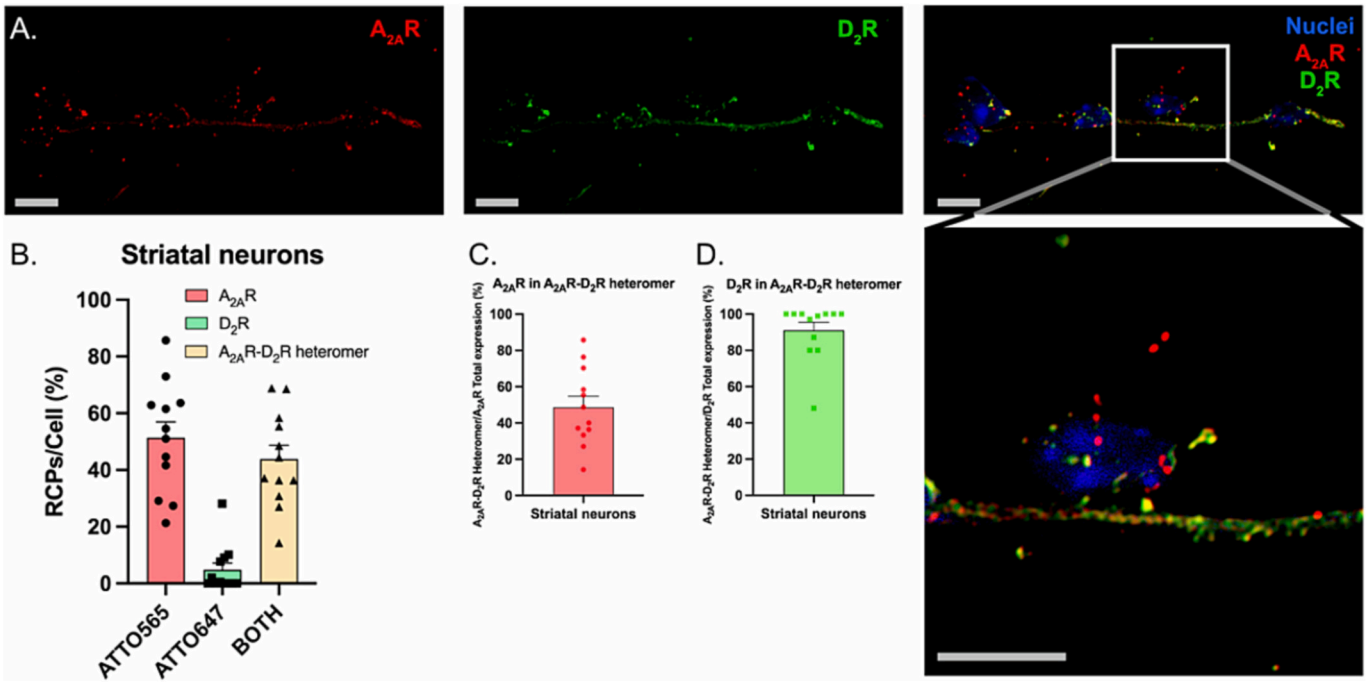

Fig. 3. MolBoolean analysis of $A_{2A}R$ and D_2R expression in mice striatal neurons. (A) Label for $A_{2A}R$ is in red, label for D_2R is in green, and label for complexes is in yellow. Hoechst staining of nuclei is shown in blue. Scale bar = 10 μm. (B) Quantification of RCPs per neuron is expressed as a percentage of the total RCPs (the sum of red, green, and yellow dots) obtained in each cell. (C) Percentage of the total $A_{2A}R$ label found in A_2R-D_2R complexes. (D) Percentage of the total D_2R label found in A_2R-D_2R complexes. Values in the bar graphs are the mean ± S.E.M. Four different experiments performed in triplicates: B) 51.3 ± 5.6 (red; $A_{2A}R$), 4.8 ± 2.4 (green; D_2R) and 43.9 ± 4.8 (yellow; A_{2A}-D_2Het); C) 48.6 ± 6.1 and D) 90.9 ± 4.5. (For interpretation of the references to colour in this figure legend, the reader is referred to the web version of this article).

containing D_2Rs was up to 49% in non-lesioned animals, and significantly increased to 70% and 74% in, respectively, lesioned and dyskinetic animals (Fig. 6 J). In these neurons the percentage of D_2Rs in heteromers was 92% in non-lesioned animals and up to 99% in dyskinetic animals (Fig. 6 K).

3. Discussion

One of the main results reported here using the novel MolBoolean technique to distinguish individual receptors from receptor complexes is that the D_2R expressed in primary neurons and in sections of the striatum of rats and non-human primates is, mainly, in complex with the $A_{2A}R$. This is a novel result, since a significant proportion of D_2Rs expressed individually or forming heteromers with receptors other than $A_{2A}R$ would have been expected. The relevant corollary is that a high percentage of D_2Rs in the MSNs of the indirect pathway are under the influence of adenosine acting on the $A_{2A}R$. This has important implications because the functionality of the heteromer consists of a regulation of the dopaminergic D_2R-mediated signaling. Adenosine reduces the affinity of dopamine for the D_2R and functional selectivity of the heteromer includes differential ß-arresting recruitment (Borroto-Escuela and Fuxe, 2019; Sahlholm et al., 2018; Surmeier et al., 2014). It is generally considered that there is antagonism within A_{2A}-D_2Het mediated by allosteric interactions within the structure of the complex, with the third intracellular loop of D_2R being a relevant actor (Fernández-Dueñas et al., 2012; Fuxe et al., 2014). Our results provide a novel context for understanding the motor effects of caffeine, a non-selective adenosine receptor antagonist. Caffeine can enter the brain and reach the striatum where it antagonizes the $A_{2A}R$; in doing so, the brake on the D_2R is released in all MSN neurons of the indirect pathway, where the dopamine receptor is expressed primarily in the form of A_{2A}-D_2Hets (Fig. 6). It should be noted that $A_{2A}R$ antagonists not only target A_{2A}-D_2Hets but also individually expressed $A_{2A}R$ and $A_{2A}Rs$ that form heteromers with other cell surface proteins (Mori, 2020).

A limitation of the study is the correlation between such a high degree of interaction between A_{2A} and D_2 receptors and the functional substrate of such a finding. Within the framework of the known adenosine/dopamine antagonistic interactions in the basal ganglia (Fuxe et al., 1998), when we discovered adenosine-dopamine receptor heteromers >20 years ago (Canals et al., 2003; Franco et al., 2001; Gines et al., 2000; Hillion et al., 2002), we thought that the heteromer was simply affecting the binding characteristics of dopamine to dopamine receptors, a result that, in the case of D_2R, had been known for years (Dasgupta et al., 1996; Díaz-Cabiale et al., 2001; Ferre et al., 1991). Later it became evident that the heteromer was not only affecting the binding of the agonist, but dopamine-receptor mediated signaling, due, at least in part, to the electrostatic interaction established between the C-terminal tail of $A_{2A}R$ and the third intracellular loop of D_2R (Navarro et al., 2010; Woods et al., 2005). The electrostatic interaction is strong and causes conformational changes that, first, affect the coupling of D_2R with G_i thereby limiting D_2R-mediated inhibition of adenylate cyclase. Furthermore, upon activation by adenosine and/or dopamine, the A_{2A}-D_2Het is desensitized and internalized as a functional unit (Fuxe et al., 2005). Our findings here suggest that disruption of the heteromer in MSNs would markedly affect the modulation by adenosine of motor control. The demonstration of this hypothesis is technically challenging but feasible by evaluating the consequences of intrastriatal injection of cell-penetrating peptides that disrupt the heteromer by inserting into the plasma membrane and altering transmembrane alpha-helical domain interactions. Peptides capable of altering the structure of the heteromer and affecting the functionality mediated by GPCR heteromers have been successfully tested in in vitro assays (Navarro et al., 2018; Perreault et al., 2016). The use of peptides able to disrupt the electrostatic interaction between the C-terminal tail of $A_{2A}R$ and the third intracellular loop of D_2R would be another option.

The finding of a proportion of $A_{2A}Rs$ that do not interact with D_2Rs in MSNs confirm that those receptors are not mediating the regulation of motor control by just interacting with D_2Rs. The detailed account on

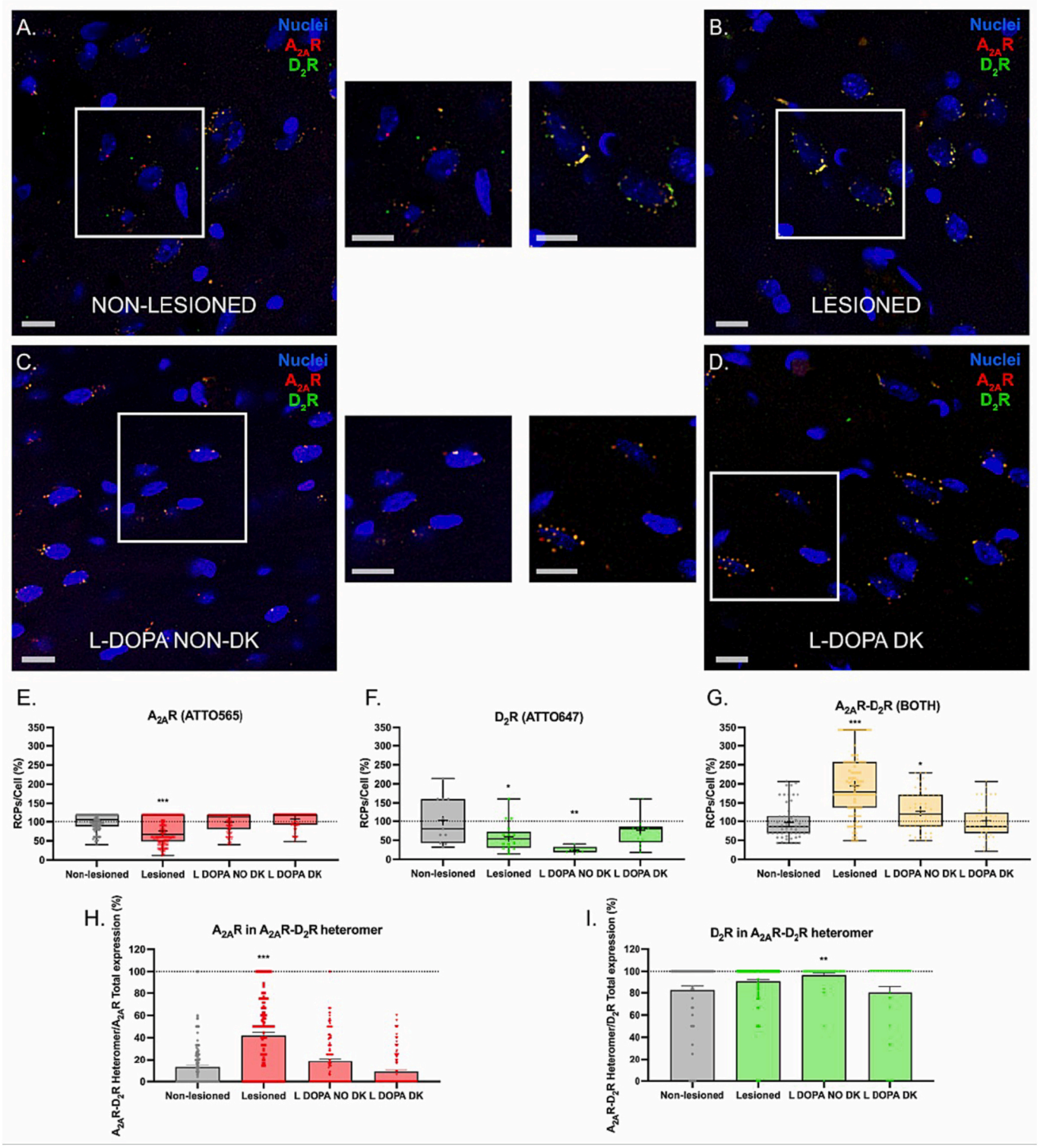

(caption on next page)

Fig. 4. MolBoolean analysis of $A_{2A}R$ and D_2R expression in striatal sections of the 6-OHDA lesioned rat PD model. MolBoolean analysis was performed in brain striatal sections of four different groups of animals: non-lesioned (A), lesioned (B), lesioned treated with L-DOPA non-dyskinetic (C) and lesioned treated with L-DOPA and dyskinetic (D). Hoechst staining of nuclei is shown in blue. Scale bar = 10 μm. Graphical representation of the expression changes of $A_{2A}R$ (E), D_2R (F) or $A_{2A}R$-D_2R complexes (G) in the four animal groups analyzed. Values were normalized by considering the RCPs per cell detected in non-lesioned animals. Data are displayed as box and whiskers plots showing the minimum and maximum values (whiskers), the first quartile, median (box lines) and mean (plus symbol) ($n = 3$, in triplicates). Cells that did not express any RCP were excluded from the analysis (*E*-G). In addition: i) cells that did not express $A_{2A}R$ RCPs were excluded from the analysis in the graph in panel E, ii) cells that did not express D_2R RCPs were excluded from the analysis in the graph in panel F, and iii) those that did not express any A_{2A}-D_2Het RCPs were excluded from the analysis in the graph in panel G. Panels H-I: Bar graphs showing the percentage of the total $A_{2A}R$ expression (H) or the total D_2R expression (I) detected as corresponding to the A_{2A}-D_2Het. Values in the bar graphs are the mean ± S.E.M. of 4 different experiments performed in triplicates: E) 100.0 ± 1.9 (non-lesioned); 75.6 ± 3.2 (lesioned); 99.2 ± 2.4 (L-DOPA no DK) and 107.0 ± 1.8 (L-DOPA DK); F) 100 ± 18.7 (non-lesioned); 59.0 ± 9.0 (lesioned); 24.5 ± 4 (L-DOPA non DK) and 75.9 ± 12.1 (L-DOPA DK); G) 100.0 ± 6.0 (non-lesioned); 194.6 ± 8.7 (lesioned); 128.3 ± 7.4 (L-DOPA no DK) and 101.1 ± 7.4 (L-DOPA DK); H) 13.1 ± 1.6 (non-lesioned); 41.9 ± 2.9 (lesioned); 18.7 ± 2.1 (L-DOPA no DK) and 9.1 ± 1.4 (L-DOPA DK); I) 82.4 ± 3.7 (non-lesioned); 90.4 ± 2.4 (lesioned); 96.7 ± 1.8 (L-DOPA no DK); 80.3 ± 5.3 (L-DOPA DK). One-way ANOVA followed by Dunnett's multiple comparison tests were used for statistical analysis. $^*p < 0.05$; $^{**}p < 0.01$; $^{***}p < 0.001$, versus non-lesioned (control) animals. ANOVA summary: E F: 33.35, $p < 0.001$; F F: 4.07, $p < 0.013$; G F: 35.72, $p < 0.001$; H F: 49.61, $p < 0.001$; I F: 4.56 $p < 0.004$. (For interpretation of the references to colour in this figure legend, the reader is referred to the web version of this article).

"*How do adenosine A_{2A} receptors regulate motor function?*" in Mori's review paper (Mori, 2020) would be consitent with the idea that those A_{2A}Rs that do not interact with the D_2R may interact with receptors for other neuromodulators, e.g. the cannabinoid CB_1 receptor (Bonaventura et al., 2014; Carriba et al., 2007). In addition, A_{2A}Rs expressed in interneurons play a role in motor control as they project to many MSNs in the direct and the indirect pathway. Electrophysiological experiments showed that effects of endocannabinoids impact on the $A_{2A}R$-mediated adenosine regulation of motor control (Tozzi et al., 2011).

It has been clearly established that the regular consumption of coffee or tea reduces the risk of suffering from idiopathic PD (Chen, 2019; Morano et al., 1994; Oñatibia-Astibia et al., 2017; Qi and Li, 2014; Ross and Petrovitch, 2001; Schwarzschild et al., 2002). Istradefylline is a selective $A_{2A}R$ antagonist that has been approved for the therapy of PD. For ethical reasons, the compound was only tested in patients taking L-DOPA. Accordingly, istradefylline was approved as adjunctive treatment to L-DOPA (Levodopa/Carbidopa) in patients PD experiencing "off" episodes (Jenner et al., 2021; Mizuno and Kondo, 2013; Sako et al., 2017). Our results indicate that an $A_{2A}R$ antagonist would counterbalance the conseequences of the increase in D_2R expression; istradefylline would lead to increase of dopaminergic signaling in the indirect pathway that could avoid the need of increasing the number of D_2Rs in the striatum of patients. Hence, it is suggested that $A_{2A}R$ blocker therapy can begin as soon as PD symptoms appear, perhaps even before the use of levodopa. Existing imaging techniques would make it possible to assess whether istradefylline administered as soon as the first clinical symptoms appear is effective in delaying the progression of the disease and/or the start of L-DOPA administration.

In the two animal PD models studied here, the level of heteromer expression changes while the predominant interaction of the D_2R with the $A_{2A}R$ persists (Figs. 4 and 6). The increase in D_2R expression has been demonstrated in caudate nucleus and putamen of parkinsonian patients (Guttman and Seeman, 1985). Therefore, the increased expression of A_{2A}-D_2Het in lesioned animals may come directly from the increased expression of dopamine receptors, that is, once synthesized, the D_2R interacts with the A_{2A}Rs that are found in large numbers in these striatal neurons. This fact fits perfectly well with the increase in the amount of $A_{2A}R$ that are forming complexes with the dopamine receptor (Figs. 4H and 6J). The sequestering of $A_{2A}R$ by the overexpressed D_2R may impact in the overall function of the $A_{2A}R$ in MSNs of the indirect pathway. One obvious consequence of increase of A_{2A}-D_2Hets in lesioned animals would be a decrease of other complexes in which the $A_{2A}R$ participates (Borroto-Escuela et al., 2014). Treatment of patients with L-DOPA reverts the increase in D_2R expression (Guttman and Seeman, 1985) a finding that fits with results in Fig. 4G, namely the attenuation of the increase of A_{2A}-D_2Hets expression after treatment of lesioned animals with L-DOPA. Valuable data could be obtained using the Molboolean-based method to assess whether the proportion of individual receptors and of heteromers varies in the 6-OHDA-lesioned PD model after administering a non-selective $A_{2A}R$ antagonist such as caffeine or a selective $A_{2A}R$ antagonist such as the one that has been approved for human use, istradefylline. Information on how the known beneficial effects of $A_{2A}R$ antagonists on both motor control and neuroprotection correlate with variations in receptor expression and A_{2A}-D_2Het proportion would be extremely valuable. Several years ago we provided data suggesting that the three receptors, A_{2A}, D_2 and CB_1 were interacting in striatal spine modules (Bonaventura et al., 2014; Ferré et al., 2009; Navarro et al., 2010, 2008; Pinna et al., 2014). Our results will hopefully boost research into the proportion of the cannabinoid receptor CB1, which may interact with A_{2A}-D_2Het. Would it be possible that a high proportion of D_2R in striatal neurons are also interacting with the CB_1 receptor? This possibility must await further development of the Molboolean technique, i.e. to be able to detect two interacting proteins using two primary antibodies of the same species (currently the technique requires to use a monoclonal -mouse- and a polyclonal -rabbit- antibody).

4. Material and methods

4.1. Cells

HEK-293 T cells, batch 70022180, were acquired from the American Type Culture Collection (ATCC). Cells were amplified and frozen in liquid nitrogen in several aliquots. Cells from each aliquot were used until passage 18. HEK-293 T cells were grown in Dulbecco's modified Eagle's medium (DMEM) (11995040; Gibco, Paisley, Scotland, UK) supplemented with 2 mM L-glutamine, 100 μg/mL sodium pyruvate, 100 U/mL penicillin/streptomycin, MEM non-essential amino acids solution (1/100) and 5% (*v*/v) heat-inactivated fetal bovine serum (FBS) (all supplements were from Invitrogen, Paisley, Scotland, UK) and maintained at 37 °C in a humid atmosphere of 5% CO_2.

4.2. Cell transfection

HEK-293 T cells were transiently transfected with the corresponding cDNA by the PEI (PolyEthylenImine; 40,872–7; Merck -Sigma_Aldrich-) method. Cells were transiently cotransfected with a constant amount of cDNA encoding for $A_{2A}R$ (2 μg) and D_2R (2 μg). Briefly, cDNAs diluted in 150 mM NaCl were mixed with PEI (5.5 mM) also prepared in 150 mM NaCl for 10 min. The cDNA-PEI complexes were transferred to HEK-293 T cells and were incubated for 4 h in a serum-starved medium. Then, the medium was replaced by a fresh supplemented culture medium, and cells were maintained at 37 °C in a humid atmosphere of 5% CO_2. 48 h after transfection, cells were washed and were treated as described in *MolBoolean experimental procedure* section.

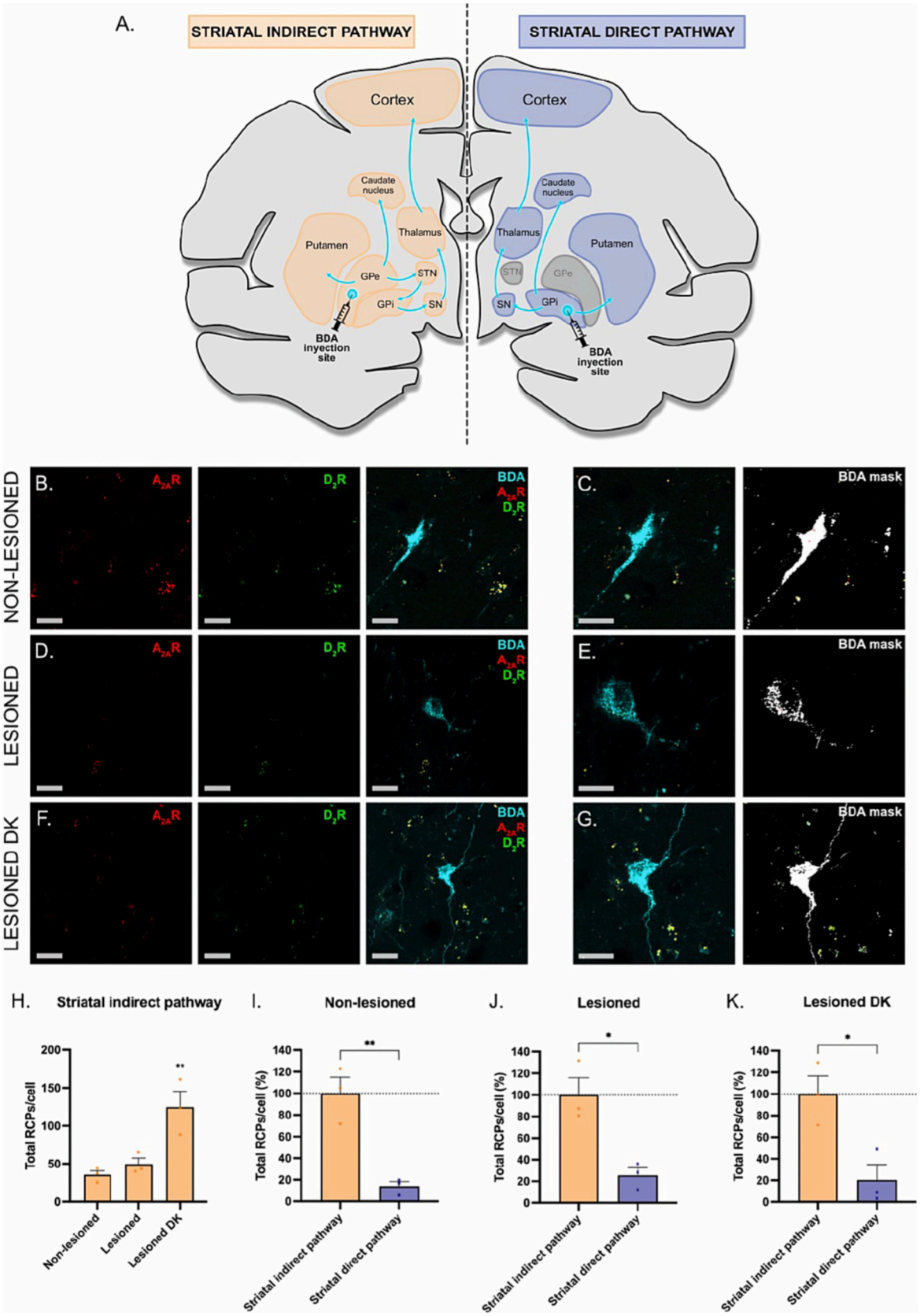

(caption on next page)

Fig. 5. MolBoolean analysis of $A_{2A}R$ and D_2R expression in brain striatal sections of the MPTP lesioned non-human primate model: BDA-labeled neurons in the indirect versus direct pathway BDA-labeled neurons. (A) A diagram depicting the site of BDA tracer injection in the primate model. To label neurons projecting in the striatal indirect pathway, BDA was injected into the external globus pallidus (GPe) (left). To detect neurons projecting in the striatal direct pathway, BDA was administered into the internal globus pallidus (GPi) (right). MolBoolean assays were performed in brain striatal sections of three different groups of animals: non-lesioned (B), lesioned (D) and lesioned dyskinetic (F). Scale bar = 10 μm. BDA in the striatal direct pathway was detected with an immunostaining with ALEXA Fluor 488-conjugated streptavidin. Only neurons that incorporated the BDA and, consequently, were stained with streptavidin-ALEXA Fluor 488 (converted to binary mask with threshold module of Cellprofiller™), were considered for the analysis of RCPs (C, E, G). Bar graphs comparing RCPs detected in BDA-labeled neurons of striatal indirect or direct pathways ($A_{2A}R$ -red- plus D_2R -green- plus A_{2A}-D_2Hets -yellow-). The comparison of data from the indirect pathway in the different groups is shown in panel H. Percentage comparing data from the indirect and direct pathways in sections from non-lesioned, lesioned and lesioned dyskinetic animals are shown in, respectively, I, J and K panels. The total number of RCPs was normalized to the mean obtained in the striatal indirect pathway for each experimental animal group. The bar graphs display the mean ± standard error of the mean (S.E.M.) of 3 independent experiments performed in triplicates: H) 35.5 ± 5.3 (non-lesioned); 49.6 ± 7.9 (lesioned); 124.7 ± 20.9 (lesioned DK); I) 100.0 ± 15.0 (indirect); 14.1 ± 4.3 (direct); J) 100.0 ± 15.9 (indirect); 25.5 ± 7.1 (direct); K) 100.0 ± 16.7 (indirect); 20.3 ± 14.4 (direct). One-way ANOVA followed by Dunnett's multiple comparison tests were used for statistical analysis in H. $^{**}p < 0.01$ (H, F: 13.05, $p < 0.014$). An unpaired two tailed *t*-test was used for statistical analysis in I—K ($^{*}p < 0.05$; $^{**}p < 0.01$). (For interpretation of the references to colour in this figure legend, the reader is referred to the web version of this article).

4.3. Isolation of primary striatal neurons

Primary striatal neurons were obtained from 19-day mouse embryos as described in (Franco et al., 2018; Hradsky et al., 2013). Cells were isolated as described in (Hradsky et al., 2013) and plated at a confluence of 40,000 cells/0.32 cm^2. Briefly, striata were dissected and digested in 0.25% trypsin for 15 min at 37 °C. Trypsinization was stopped by repeated washes with Hank's Buffered Saline Solution (HBSS, Gibco). Cells were brought to a single cell suspension by repeated pipetting followed by passage through a 100 μm-pore mesh. Cells were then resuspended in supplemented DMEM and seeded on glass coverslips at a density of 3.5×10^5 cells/mL in twelve-well plates for MolBoolean assays. The day after, medium was replaced by neurobasal medium supplemented with 2 mM L-glutamine, 100 U/mL penicillin/streptomycin, and 2% (v/v) B27 (10889038; Gibco) and culture was maintained for 12 days. Cultures were maintained at 37 °C in a 5% CO_2 humid atmosphere. Immunodetection of specific NeuN marker (ab190195; 1:200; Abcam) showed that preparations contained >98% neurons.

4.4. Rat PD model generation, levodopa treatment, and dyskinesia assessment

All experiments were carried out in accordance with EU directives (2010/63/EU and 86/609/CEE). The rat study protocol was approved by the corresponding committee at the University of Santiago de Compostela (protocol 14715012/2021/012; last revision 16 April 2021). Details of unilateral 6-hydroxydopamine (6-OHDA)-based PD rat model generation and behavioral analysis are given elsewhere (Lopez-Lopez et al., 2020). Animal selection was made upon performance in the amphetamine rotation test (Muñoz et al., 2014); rats that displayed >6 full body turns/min ipsilateral to the lesion were included in the study. Of the animals selected (18 in total), 12 were chronically treated with L-DOPA daily for 3 weeks and 6 with vehicle instead of L-DOPA. A mixture of L-DOPA methyl ester (6 mg/kg) plus benserazide (10 mg/kg) was administered subcutaneously. The treatment induces dyskinetic movements in some rats. Abnormal involuntary movements were evaluated according to the rat dyskinesia scale described in a previous report (Farré et al., 2015). The severity of each abnormal involuntary movement (AIM) subtype (limb, orolingual, and axial) was assessed using scores from 0 to 4 (1 = occasional, present <50% of the time; 2 = frequent, present >50% of the time; 3 = continuous but interrupted by strong sensory stimuli; 4 = continuous, not interrupted by strong sensory stimuli). Rats were classified as "dyskinetic" if they displayed a score ≥ 2 per monitoring period on at least two AIM subtypes. Animals classified as "non-dyskinetic" exhibited either no L-DOPA-induced abnormal involuntary movements or very mild/occasional ones. Animals with low scores, either non-dyskinetic or dyskinetic, were excluded. In summary, four groups of animals were obtained: [1] non-lesioned [2] lesioned, treated with vehicle; [3] lesioned and became dyskinetic when treated with L- DOPA; and [4] lesioned and did not become dyskinetic upon L-DOPA treatment. Overall, 4 animals (those with better scores) were selected in each of the following 4 groups: non-lesioned, lesioned, lesioned/L-DOPA non-dyskinetic, and lesioned/L-DOPA dyskinetic. The MolBoolean assays (see below) was performed in different fields of striatal sections from the 16 selected animals. The striatum was delimited in sections using a bright field, and images were captured within delimitation coordinates. Images were taken in the ipsilateral hemisphere.

4.5. Macaca fascicularis PD model

A total of six young adult male *M. fascicularis* primates (body weight 3.5–4.7 kg) were used in this study. Animal handling was conducted in accordance with the European Council Directive 2010/63/UE as well as in keeping with current Spanish legislation (RD53/2013). The experimental design was reviewed and approved by the Ethical Committee for Animal Testing of the University of Navarra (protocol ref.: 009/12). All animals were captive-bred and supplied by R.C. Hartelust (Leiden, the Netherlands).

The stereotaxic atlas of Lanciego and Vázquez (Lanciego and Vázquez, 2012) was used to allocate proper coordinates of tracer injection into the internal and external divisions of the globus pallidus (GPi and GPe, respectively). Target selection was assisted by ventriculography, ensuring appropriate targeting of either the GPi or GPe. Coordinates for the GPi nucleus were 3.5 mm caudal to the anterior commissure (ac), 1.5 mm ventral to the bicommisural plane (ac-pc plane), and 6 mm lateral to the midline. Coordinates for the GPe nucleus were 3.5 mm caudal to ac, 1.5 mm dorsal to the ac-pc plane, and 8.5 mm lateral to the mid-line. Animals received a single pressure injection of 1 μL of biotinylated dextran amine (BDA; 10 kDa, lysine fixable; D-1956, Molecular Probes, Invitrogen) through a Hamilton syringe (5 mg/mL in 0.01 M phosphate buffer (PB) at neutral pH) in either the GPi or the GPe nuclei. Tracer delivery was carried out in pulses of 0.1 μL/2 min and once completed, the microsyringe was left in place for additional 15 min before withdrawal to minimize tracer reflux through the injection tract. The tracing time should be adapted to the length of the pathway being studied. There is little information available on the detectability of BDA as a function of its persistence time, but it seems that it has a wide range (Brandt and Apkarian, 1992; Lanciego et al., 1998a; Lanciego et al., 1998b; Rajakumar et al., 1993; Veenman et al., 1992; Wouterlood and Jorritsma-Byham, 1993). The BDA's longest reported tracing time is 7 weeks for squirrel monkeys. In our case, 2 weeks were enough to obtain consistent staining.

Two weeks post injection, animals were anesthetized with an overdose of anesthesia and perfused transcardially. The perfusates were made of a saline Ringer's solution followed by 3000 mL of a fixative solution containing 4% paraformaldehyde and 0.1% glutaraldehyde in 0.125 M PB at neutral pH. Perfusion was continued with 1000 mL of a cryoprotectant solution made of 10% glycerin and 1% of dimethyl sulfoxide (DMSO) in 0.125 M PB, pH 7.4. Once perfusion was completed,

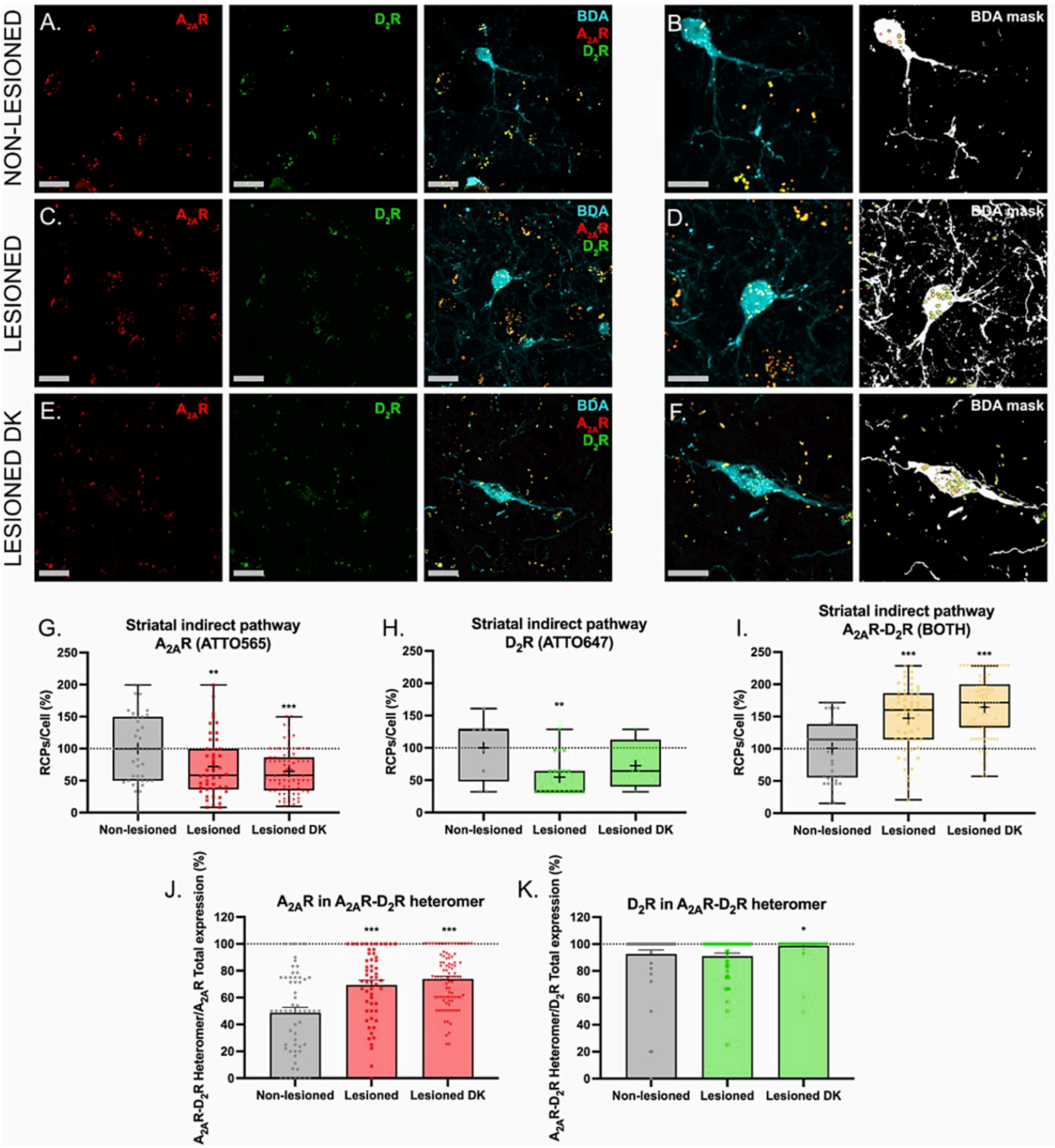

Fig. 6. MolBoolean analysis of $A_{2A}R$ and D_2R expression in brain striatal sections of the MPTP lesioned non-human primate model: Focus on neurons of the indirect pathway. MolBoolean assays were performed in brain striatal sections of three different groups of animals: non-lesioned (A), lesioned (C) and lesioned dyskinetic (E). Scale bar = 10 μm. BDA-containing neurons originated from BDA injections in the GPe, were detected using with ALEXA Fluor 488-conjugated streptavidin (Light blue; B—F). Only neurons that incorporated the BDA and, consequently, were stained with ALEXA Fluor 488-conjugated streptavidin (converted to binary mask with threshold module of CellProfiler™), were considered for the analysis of RCPs. Graphical representation of the expression changes of $A_{2A}R$ (G), D_2R (H) or $A_{2A}R$-D_2R complexes (I) in the three animal groups analyzed. Values were normalized as percentage of RCPs per neuron detected in non-lesioned animals. Data are displayed as box and whiskers plots showing the minimum and maximum points (whiskers), the first quartile, median (box lines) and mean (plus symbol) ($n = 3$, in triplicates). Neurons that were analyzed and did not express any RCP were excluded from the graphs (G-I). In addition, cells that did not express free $A_{2A}R$ RCPs were excluded from (G), those that did not express free D_2R RCPs from (H) and those that did not express any $A_{2A}R$-D_2R complex from (I). Bar graphs show the percentage of the total $A_{2A}R$ expression (J) or the total D_2R expression (K) detected A_{2A}-D_2Het RCPs. Values in the bar graphs are the mean ± S.E.M. of 3 different experiments performed in triplicates: G) 100.0 ± 7.3 (non-lesioned); 72.1 ± 7.0 (lesioned); 64.8 ± 4.0 (lesioned DK); H) 100.0 ± 15.6 (non-lesioned); 54.6 ± 6.6 (lesioned); 72.3 ± 20.2 (lesioned DK); I) 100.0 ± 7.1 (non-lesioned); 147.5 ± 6.8 (lesioned); 164.5 ± 4.8 (lesioned DK); J) 48.7 ± 4.0 (non-lesioned); 69.5 ± 3.5 (lesioned); 73.8 ± 2.1 (lesioned DK); K) 92.6 ± 2.9 (non-lesioned); 91.1 ± 2.1 (lesioned); 98.8 ± 1.7 (lesioned DK). One-way ANOVA followed by Dunnett's multiple comparison tests were used for statistical analysis. *$p < 0.05$; **$p < 0.01$; ***$p < 0.001$, versus non-lesioned treatment. ANOVA summary: G F: 10.17, $p < 0.001$; H F: 4.92, $p < 0.014$; I F: 26.78, $p < 0.001$; J F: 18.94, $p < 0.001$; K F: 5.786 $p < 0.004$. (For interpretation of the references to colour in this figure legend, the reader is referred to the web version of this article).

the brain was removed and stored in a cryoprotective solution containing 20% glycerin and 2% DMSO for 48–72 h. Finally, 10 series of frozen coronal adjacent sections (40-μm thick) were obtained in a sliding microtome. These series were used for Molboolean assays.

The remaining two series of sections were stored at −80 °C as backup materials for further processing, if needed. Detection of transported BDA was carried out by 60 min of incubation in ALEXA488-conjugated streptavidin (1:100; S32354; ThermoFisher).

4.6. MolBoolean experimental procedure

The MolBoolean assay kit was obtained from Atlas Antibodies (Stockholm, Sweden) and the manufacturer's protocol was followed. The protocol supplied by Atlas Antibodies is based on that recently reported by (Raykova et al., 2022).

Cells (HEK-293 T transfected cells or striatal neurons) or brain slices (rat or non-human primate PD model) washed using PBS were fixed with ice-cold 4% formalin solution (1004969011; Merck -Sigma_Aldrich-) for 15 min. Samples were washed 3 times with PBS and permeabilized with TBS (ThermoFisher Scientific) 0.2% *v*/v Triton X-100 (142314.1611; Panreac) for 15 min (cells) or 30 min (brain slices). After washing for 2 min with TBS, the samples were transferred to a humid chamber. The samples in glass microscope slides (SuperFrost®Plus; ref. 631–0108; VWR) were delimitated with the hydrophobic barrier of A-PAP Pen (Z672548; Merck). Blocking was done with Intercept Blocking Buffer (927–700001; LI-COR) for 1 h at 37 °C. The samples were incubated with a mouse monoclonal anti-A_{2A}R primary antibody (1:250; 05–717; Millipore -Merck-) for 2 h at RT, followed by 3 min wash in TBS. Afterwards samples were incubated (overnight at 4 °C) with a rabbit polyclonal anti-D_2R primary antibody (1:75; AB5084P; Merck). Primary antibodies were diluted in blocking buffer. The samples were then washed 3 times (3 min each) with 0.05% TBS-Tween20 (TBST; P5927; Merck -Sigma_Aldrich-) and incubated (for 1 h at 37 °C) with 3 μg/mL of each proximity probe (A and B), diluted in intercept blocking buffer. Next, samples were washed once during 3 mins with in HBS-Tween20 (HSBT) and twice during 3 mins min in TBST. Subsequently, the cells were incubated (1 h at 37 °C) with 0.05 μM oligonucleotide sequence in T4 DNA ligase buffer supplemented with 0.25 mg/mL BSA (Merck -Sigma_Aldrich-), followed by a 3 min wash with HBST and a 3 min wash with TBST. Later, a mix of 0.125 U/μL Nt.*Bsm*AI (nickase enzyme) in NEBuffer CutSmart (New England Biolabs) and 0.25 mg/mL BSA was added (30 min at 37 °C). For the hybridization of the tag oligonucleotides, the samples washed with TBST and then were incubated (1 h at 37 °C) in TBS, 0.25 mg/mL BSA and 0.5 μM tag oligonucleotides A and B. Finally, ligation was achieved using 0.05 U/μL T4 ligase in T4 DNA ligase buffer containing 0.25 mg/mL BSA (1 h at 37 °C). Washed samples were incubated (90 min at 37 °C) in phi29 polymerase buffer (Monserate Biotechnology group; San Diego, CA), 0.25 mg/mL BSA, 1.25 mM dNTPs (Thermo Fisher Scientific), and 1 U/μL phi29 polymerase (Monserate Biotechnology group). Further washes with TBST preceded incubation (1 h at 37 °C) with detection mix (0.025 μM detection oligonucleotides A and B dissolved in TBS). Excess reagent was removed using HSB and later, TBS.

Finally, to mitigate autofluorescence in the brain slices, samples were treated with the Tissue Autofluorescence Quenching Kit (R37630; ThermoFisher). Nuclear counterstaining was conducted using *Hoechst*33342 dye (1:100; ThermoFisher) for 5 min. Slides were mounted with Shandon™ Immu-Mount™ (9990402; ThermoFisher) and sealed with cover glass #1.5 (2980–244; Corning). Samples were observed in a Zeiss 880 confocal microscope (Carl Zeiss, Oberkochen, Germany) equipped with an apochromatic 63× oil immersion objective (N.A. 1.4) and 405, 488, 561 and 640 nm laser lines. For each field of view, a stack of three or four channels (405 nm for nuclei in blue, 561 nm for A_{2A}R in red and 640 nm for D_2R in green with or without 488 nm for BDA in light blue) and images from a minimum of 5 Z stacks with a step size of 0.5 μm were acquired.

4.7. Data analysis

Quantification and colocalization analyses of the RCPs were performed with specifically designed pipelines for the CellProfiler™ software on the deconvolved but otherwise unaltered images. Images were deconvolved with Parallel Spectral Deconvolution v1.12 plugin for ImageJ software applying the Tikhonov's algorithm, after calculating the appropriate Point Spread Function (PSF) by considering the refraction index of the mounting medium, numerical aperture of the objective and wavelength of the channel for deconvolution.

Deconvolved split-channel images in grayscale format were analyzed using the CellProfiler™ software version 5.2.5. For MolBoolean images analysis, a pipeline for RCPs quantification, with slight modifications between assays to adjust the size for nuclei detection or the estimated area of each cell, was compiled with the following modules: *IdentifyPrimaryObjects, IdentifySecondaryObjects, EnhanceOrSuppressFeatures, GaussianFilter, IdentifyPrimaryObjects, ExpandOrShrinkObjects, IdentifySecondaryObjects, CombineObjects, MaskObjects, MeasureObjectIntensity, ClassifyObjects, FilterObjects, OverlayOutlines, SaveImages, RelateObjects,* and *ExportToSpreadsheet.*

First, *IdentifyPrimaryObjects* was used on the Hoechst stain channel (blue; ch00) to identify nuclei based on their typical diameter measured in pixels and the application of two-class Otsu thresholding. Next, *IdentifySecondaryObjects* module was used to identify the cells, by means of expanding the nuclei by distance. *GaussianFilter* module was used with low sigma value to effectively reduce noise, preserving fine details but improving image quality for subsequent RCPs analysis on ATTO565 (red; ch01) and ATTO647 (green; ch02) channels. Then, the *EnhanceOrSupressFeatures* module was used to improve specks (RCPs) and the *IdentifyPrimaryObjects* module to quantify RCPs of a specific diameter in pixels unit. The *ExpandOrShrinkObjects* module was used to shrink objects to a single point, while the *IdentifySecondaryObjects* module was used to optimize RCPs delimitation. With the new RCPs definition, the *CombineObjects* module merged all blobs in ch01 and ch02 channels and *MaskObjects* excluded from the analysis all the RCPs outside previously defined cells. The intensity of the RCPs in ch01 and ch02 channels was determined with the *MeasureObjectIntensity* module and, with the *ClassifyObjects* module; identified RCPs were classified as background (low intensity for both channels), as A_{2A}R RCPs (high intensity for ATTO565, low intensity for ATTO647), as D_2R RCPs (low intensity for ATTO565, high intensity for ATTO647) or as A_{2A}R-D_2R heteromer RCPs (high intensity for both channels). RCPs were then filtered with the *FilterObjects* module, in A_{2A} or D_2 free receptors or in A_{2A}-D_2 receptor complexes, with the option of saving this information in an image using *OverlayOutlines* and *SaveImages* modules. Afterwards, with the RCPs were matched to their appropriate cell using the *RelateObjects* module. Finally, all data collected from the execution of the pipeline was exported to a .CSV file using the *ExportToSpreadsheet* module.

Several modifications were required to the above-described pipeline to facilitate MolBoolean quantification in non-human primate samples. The main purpose was to quantify RCPs exclusively in neurons that had incorporated the BDA tracer. To achieve it, the *Threshold* module was used to convert ALEXA488 channel (ch03) into a binary image and for automatic structure segmentation using the minimum cross-entropy thresholding method. After that, the *MaskImage* module was used to generate new images for ch01 and ch02 channels containing only the RCPs enclosed in the mask generated with the *Threshold* module. Quality control of the segmentation was performed with the *SaveImages* module.

Corrections of brightness and contrast were made on figure images to improve the visibility of RCPs. Pseudo-coloring was applied to all images; Hoechst33342, ALEXA488, ATTO565, and ATTO647, are depicted, respectively, in blue, light blue, red and green.

4.8. Immunocytochemistry

HEK-293 T cells were seeded on glass coverslips in 12-well plates.

Twenty-four hours later, cells were transfected with cDNA for human D_2R. Forty-eight hours after transfection, cells were fixed in 4% paraformaldehyde for 15 min and washed twice with PBS containing 20 mM glycine before permeabilization with PBS-glycine containing 0.2% Triton X-100 (15 min incubation). Blocking was performed with PBS containing 1% bovine serum albumin (1 h). Untransfected and transfected cells were incubated (1 h) with a rabbit anti-D_2R antibody (1:100, AB5084P; Merck) and subsequently incubated (1 h) with a Cy3-conjugated anti-rabbit IgG secondary antibody (1:200, 711–166-152 (red), Jackson ImmunoResearch, St. Thomas Place, UK). Nuclei were stained with Hoechst (1:100 from 1 mg/mL stock solution). Samples were washed several times and mounted with Immu-mount® (FisherScientific). Images were obtained in a Zeiss LSM 880 confocal microscope (ZEISS, Germany) using the 63× oil objective. Images are shown in Supplementary Fig. S1.

4.9. Statistical analysis

The data in graphs are expressed as mean ± standard error of the mean (SEM) ($n \geq 5$). GraphPad Prism 9.5 software (San Diego, CA, USA) was used for data fitting and statistical analysis. Multiple group comparisons were performed by one-way ANOVA followed by Dunnett's *post-hoc* test. Unpaired two-tailed Student's *t*-test was used for comparisons between two groups. Significant differences were considered when the p value was <0.05.

Author contributions

RF, RRS and GN designed the project. JLG, AM and AIR produced the rodent model of PD, did the pharmacological treatment and performed the behavioral experiments. JLL and AR produced the monkey model of PD, did the injection of the BDA tracer and provided the striatal slices. RRS, GN and IRR participated in cell culture, obtention of primary cultures, staining using the MolBoolean technique and confocal imaging. RRS did the Boolean analysis of the data and constructed the figs. RF and RRS wrote the first draft. All co-authors edited the manuscript and approved the submitted version.

Funding

This work was supported by grants PID2021-126848NB-I00 (JLG), PID2020-120308RB-I00 (JLL), PID 2020-113430RB-I00 (GN) and PID 2021-126600OB-I00 (RF) funded by Spanish MCIN/AEI/10.13039/ 550 501100011033 and, as appropriate, by "ERDF A way of making Europe," by the "European Union" or by the "European Union Next-Generation EU/PRTR." The research group of the University of Barcelona is considered of excellence (grup consolidat #2021 SGR 554 00304) by the Regional Catalonian Government. RRS has been awarded a Juan de la Cierva "training" contract.

Declaration of Competing Interest

Authors declare no conflict of interest.

Data availability

Data will be made available on request.

Appendix A. Supplementary data

Supplementary data to this article can be found online at https://doi.org/10.1016/j.nbd.2023.106341.

References

Alexander, S.P., Christopoulos, A., Davenport, A.P., Kelly, E., Mathie, A., Peters, J.A., Veale, E.L., Armstrong, J.F., Faccenda, E., Harding, S.D., Pawson, A.J., Southan, C., Davies, J.A., Abbracchio, M.P., Alexander, W., Al-hosaini, K., Bäck, M., Barnes, N.M., Bathgate, R., Beaulieu, J.-M., Bernstein, K.E., Bettler, B., Birdsall, N.J.M., Blaho, V., Boulay, F., Bousquet, C., Bräuner-Osborne, H., Burnstock, G., Caló, G., Castaño, J.P., Catt, K.J., Ceruti, S., Chazot, P., Chiang, N., Chini, B., Chun, J., Cianciulli, A., Civelli, O., Clapp, L.H., Couture, R., Csaba, Z., Dahlgren, C., Dent, G., Singh, K.D., Douglas, S.D., Dournaud, P., Eguchi, S., Escher, E., Filardo, E.J., Fong, T., Fumagalli, M., Gainetdinov, R.R., de Gasparo, M., Gerard, C., Gershengorn, M., Gobeil, F., Goodfriend, T.L., Goudet, C., Gregory, K.J., Gundlach, A.L., Hamann, J., Hanson, J., Hauger, R.L., Hay, D.L., Heinemann, A., Hollenberg, M.D., Holliday, N. D., Horiuchi, M., Hoyer, D., Hunyady, L., Husain, A., IJzerman, A.P., Inagami, T., Jacobson, K.A., Jensen, R.T., Jockers, R., Jonnalagadda, D., Karnik, S., Kaupmann, K., Kemp, J., Kennedy, C., Kihara, Y., Kitazawa, T., Kozielewicz, P., Kreienkamp, H.-J., Kukkonen, J.P., Langenhan, T., Leach, K., Lecca, D., Lee, J.D., Leeman, S.E., Leprince, J., Li, X.X., Williams, T.L., Lolait, S.J., Lupp, A., Macrae, R., Maguire, J., Mazella, J., McArdle, C.A., Melmed, S., Michel, M.C., Miller, L.J., Mitolo, V., Mouillac, B., Müller, C.E., Murphy, P., Nahon, J.-L., Ngo, T., Norel, X., Nyimanu, D., O'Carroll, A.-M., Offermanns, S., Panaro, M.A., Parmentier, M., Pertwee, R.G., Pin, J.-P., Prossnitz, E.R., Quinn, M., Ramachandran, R., Ray, M., Reinscheid, R.K., Rondard, P., Rovati, G.E., Ruzza, C., Sanger, G.J., Schöneberg, T., Schulte, G., Schulz, S., Segaloff, D.L., Serhan, C.N., Stoddart, L.A., Sugimoto, Y., Summers, R., Tan, V.P., Thal, D., Thomas, W. Wally, Timmermans, P.B.M.W.M., Tirupula, K., Tulipano, G., Unal, H., Unger, T., Valant, C., Vanderheyden, P., Vaudry, D., Vaudry, H., Vilardaga, J.-P., Walker, C.S., Wang, J.M., Ward, D.T., Wester, H.-J., Willars, G.B., Woodruff, T.M., Yao, C., Ye, R.D., 2021. The concise guide to pharmacology 2021/22: G protein-coupled receptors. Br. J. Pharmacol. 178, S27–S156. https://doi.org/10.1111/BPH.15538.

Antonelli, T., Fuxe, K., Agnati, L., Mazzoni, E., Tanganelli, S., Tomasini, M.C., Ferraro, L., 2006. Experimental studies and theoretical aspects on A2A/D2 receptor interactions in a model of Parkinson's disease. Relevance for L-dopa induced dyskinesias. J. Neurol. Sci. 248, 16–22. https://doi.org/10.1016/J.JNS.2006.05.019.

Beggiato, S., Tomasini, M.C., Borelli, A.C., Borroto-Escuela, D.O., Fuxe, K., Antonelli, T., Tanganelli, S., Ferraro, L., 2016. Functional role of striatal A2A, D2, and mGlu5 receptor interactions in regulating striatopallidal GABA neuronal transmission. J. Neurochem. 138, 254–264. https://doi.org/10.1111/JNC.13652.

Bonaventura, J., Rico, A.J., Moreno, E., Sierra, S., Sánchez, M., Luquin, N., Farré, D., Müller, C.E., Martínez-Pinilla, E., Cortés, A., Mallol, J., Armentero, M.-T., Pinna, A., Canela, E.I., Lluís, C., McCormick, P.J., Lanciego, J.L., Casadó, V., Franco, R., 2014. L-DOPA-treatment in primates disrupts the expression of a(2A) adenosine-CB(1) cannabinoid-D(2) dopamine receptor heteromers in the caudate nucleus. Neuropharmacology 79, 90–100. https://doi.org/10.1016/j.neuropharm.2013.10.036.

Borroto-Escuela, D.O., Fuxe, K., 2019. Adenosine heteroreceptor complexes in the basal ganglia are implicated in Parkinson's disease and its treatment. J. Neural Transm. https://doi.org/10.1007/s00702-019-01969-2.

Borroto-Escuela, D.O., Brito, I., Romero-Fernandez, W., Di Palma, M., Oflijan, J., Skieterska, K., Duchou, J., Van Craenenbroeck, K., Suárez-Boomgaard, D., Rivera, A., Guidolin, D., Agnati, L.F., Fuxe, K., 2014. The G protein-coupled receptor heterodimer network (GPCR-HetNet) and its hub components. Int. J. Mol. Sci. 15, 8570–8590. https://doi.org/10.3390/ijms15058570.

Brandt, H.M., Apkarian, A.V., 1992. Biotin-dextran: a sensitive anterograde tracer for neuroanatomic studies in rat and monkey. J. Neurosci. Methods 45, 35–40. https://doi.org/10.1016/0165-0270(92)90041-B.

Canals, M., Marcellino, D., Fanelli, F., Ciruela, F., De Benedetti, P., Goldberg, S.R., Neve, K., Fuxe, K., Agnati, L.F., Woods, A.S., Ferré, S., Lluis, C., Bouvier, M., Franco, R., 2003. Adenosine A2A-dopamine D2 receptor-receptor heteromerization: qualitative and quantitative assessment by fluorescence and bioluminescence energy transfer. J. Biol. Chem. 278, 46741–46749. https://doi.org/10.1074/jbc.M306451200.

Carriba, P., Ortiz, O., Patkar, K., Justinova, Z., Stroik, J., Themann, A., Müller, C., Woods, A.S., Hope, B.T., Ciruela, F., Casadó, V., Canela, E.I., Lluis, C., Goldberg, S.R., Moratalla, R., Franco, R., Ferré, S., 2007. Striatal adenosine A2A and cannabinoid CB1 receptors form functional Heteromeric complexes that mediate the motor effects of cannabinoids. Neuropsychopharmacology 32, 2249–2259. https://doi.org/10.1038/sj.npp.1301375.

Chen, J.-F., 2019. CHAPTER 7. Caffeine and Parkinson's Disease: From molecular targets to epidemiology and clinical trials. In: Coffee. Royal Society of Chemistry, pp. 171–195. https://doi.org/10.1039/9781788015028-00171.

Chen, J.F., Moratalla, R., Impagnatiello, F., Grandy, D.K., Cuellar, B., Rubinstein, M., Beilstein, M.A., Hackett, E., Fink, J.S., Low, M.J., Ongini, E., Schwarzschild, M.A., 2001. The role of the D(2) dopamine receptor (D(2)R) in A(2A) adenosine receptor (A(2A)R)-mediated behavioral and cellular responses as revealed by A(2A) and D(2) receptor knockout mice. Proc. Natl. Acad. Sci. U. S. A. 98, 1970–1975. https://doi.org/10.1073/PNAS.98.4.1970.

Dasgupta, S., Ferré, S., Kull, B., Hedlund, P.B., Finnman, U.B., Ahlberg, S., Arenas, E., Fredholm, B.B., Fuxe, K., 1996. Adenosine A2A receptors modulate the binding characteristics of dopamine D2 receptors in stably cotransfected fibroblast cells. Eur. J. Pharmacol. 316, 325–331.

Díaz-Cabiale, Z., Hurd, Y., Guidolin, D., Finnman, U.B., Zoli, M., Agnati, L.F., Vanderhaeghen, J.J., Fuxe, K., Ferré, S., 2001. Adenosine A2A agonist CGS 21680 decreases the affinity of dopamine D2 receptors for dopamine in human striatum. Neuroreport 12, 1831–1834. https://doi.org/10.1097/00001756-200107030-00014.

Daniel Farré, Ana Muñoz, Estefanía Moreno, Irene Reyes-Resina, Júlia Canet-Pons, Iria G. Dopeso-Reyes, Alberto J. Rico, Carme Lluís, Josefa Mallol, Gemma Navarro, Enric I. Canela, Antonio Cortés, José L. Labandeira-García, Vicent Casadó, José L. Lanciego, Rafael Franco (2015). Stronger Dopamine D1 Receptor-Mediated Neurotransmission in Dyskinesia. Mole. Neurobiol. 52, 1408–1420. doi: 10.1007/s12035-014-8936-x. PMID: 25344317.

Feltmann, K., Borroto-Escuela, D.O., Rüegg, J., Pinton, L., de Oliveira Sergio, T., Narváez, M., Jimenez-Beristain, A., Ekström, T.J., Fuxe, K., Steensland, P., 2018. Effects of long-term alcohol drinking on the dopamine D2 receptor: gene expression and Heteroreceptor complexes in the striatum in rats. Alcohol. Clin. Exp. Res. 42, 338–351. https://doi.org/10.1111/ACER.13568.

Fernández-Dueñas, V., Gómez-Soler, M., Jacobson, K.A., Kumar, S.T., Fuxe, K., Borroto-Escuela, D.O., Ciruela, F., 2012. Molecular determinants of A2AR-D2R allosterism: role of the intracellular loop 3 of the D2R. J. Neurochem. 123, 373–384. https://doi.org/10.1111/J.1471-4159.2012.07956.X.

Ferre, S., von Euler, G., Johansson, B., Fredholm, B.B., Fuxe, K., 1991. Stimulation of high-affinity adenosine A2 receptors decreases the affinity of dopamine D2 receptors in rat striatal membranes. Proc. Natl. Acad. Sci. U. S. A. 88, 7238–7241.

Ferre, S., O'Connor, W.T., Fuxe, K., Ungerstedt, U., 1993. The striopallidal neuron: a main locus for adenosine-dopamine interactions in the brain. J. Neurosci. 13, 5402–5406. https://doi.org/10.1523/JNEUROSCI.13-12-05402.1993.

Ferré, S., Popoli, P., Giménez-Llort, L., Rimondini, R., Müller, C.E., Strömberg, I., Ögren, S.O., Fuxe, K., 2001. Adenosine/dopamine interaction: implications for the treatment of Parkinson's disease. Parkinsonism Relat. Disord. 7, 235–241. https://doi.org/10.1016/S1353-8020(00)00063-8.

Ferré, S., Goldberg, S.R., Lluis, C., Franco, R., 2009. Looking for the role of cannabinoid receptor heteromers in striatal function. Neuropharmacology 56, 226–234. https://doi.org/10.1016/j.neuropharm.2008.06.076.

Franco, R., Ferré, S., Agnati, L., Torvinen, M., Ginés, S., Hillion, J., Casadó, V., Lledó, P. M., Zoli, M., Lluis, C., Fuxe, K., 2000. Evidence for adenosine/dopamine receptor interactions: indications for heteromerization. Neuropsychopharmacology 23, S50–S59. https://doi.org/10.1016/S0893-133X(00)00144-5.

Franco, R., Ferré, S., Torvinen, M., Ginés, S., Hillion, J., Ciruela, F., Canela, E.I., Mallol, J., Casadó, V., Lluis, C., Fuxe, K., 2001. Adenosine/dopamine receptor-receptor interactions in the central nervous system. Drug Dev. Res. 52, 296–302. https://doi.org/10.1002/ddr.1127.

Franco, R., Aguinaga, D., Reyes, I., Canela, E.I., Lillo, J., Tarutani, A., Hasegawa, M., Del Ser-Badia, A., del Rio, J.A., Kreutz, M.R., Saura, C.A., Navarro, G., 2018. N-methyl-D-aspartate receptor link to the MAP kinase pathway in cortical and hippocampal neurons and microglia is dependent on calcium sensors and is blocked by α-Synuclein, tau, and Phospho-tau in non-transgenic and transgenic APPSw, Ind Mice. Front. Mol. Neurosci. 11, 273. https://doi.org/10.3389/fnmol.2018.00273.

Fuxe, K., Ferré, S., Zoli, M., Agnati, L.F., 1998. Integrated events in central dopamine transmission as analyzed at multiple levels. Evidence for intramembrane adenosine a (2A)/dopamine D2and adenosine A1/dopamine D1receptor interactions in the basal ganglia. Brain Res. Rev. 26, 258–273. https://doi.org/10.1016/S0165-0173(97)00049-0.

Fuxe, K., Ferré, S., Canals, M., Torvinen, M., Terasmaa, A., Marcellino, D., Goldberg, S.R., Staines, W., Jacobsen, K.X., Lluis, C., Woods, A.S., Agnati, L.F., Franco, R., 2005. Adenosine a_{2A} and dopamine D₂ Heteromeric receptor complexes and their function. J. Mol. Neurosci. 26, 209–220. https://doi.org/10.1385/JMN:26:2-3:209.

Fuxe, K., Ferré, S., Genedani, S., Franco, R., Agnati, L.F., 2007. Adenosine receptor-dopamine receptor interactions in the basal ganglia and their relevance for brain function. Physiol. Behav. 92, 210–217. https://doi.org/10.1016/j.physbeh.2007.05.034.

Fuxe, K., Tarakanov, A., Romero Fernandez, W., Ferraro, L., Tanganelli, S., Filip, M., Agnati, L.F., Garriga, P., Diaz-Cabiale, Z., Borroto-Escuela, D.O., 2014. Diversity and Bias through receptor-receptor interactions in GPCR Heteroreceptor complexes. Focus on examples from dopamine D2 receptor Heteromerization. Front. Endocrinol. (Lausanne) 5, 1–11. https://doi.org/10.3389/fendo.2014.00071.

Gines, S., Hillion, J., Torvinen, M., Le Crom, S., Casado, V., Canela, E.I., Rondin, S., Lew, J.Y., Watson, S., Zoli, M., Agnati, L.F., Verniera, P., Lluis, C., Ferre, S., Fuxe, K., Franco, R., 2000. Dopamine D1 and adenosine A1 receptors form functionally interacting heteromeric complexes. Proc. Natl. Acad. Sci. 97, 8606–8611. https://doi.org/10.1073/pnas.150241097.

Guttman, M., Seeman, P., 1985. L-dopa reverses the elevated density of D2 dopamine receptors in Parkinson's diseased striatum. J. Neural Transm. 64, 93–103. https://doi.org/10.1007/BF01245971.

Hillion, J., Canals, M., Torvinen, M., Casado, V., Scott, R., Terasmaa, A., Hansson, A., Watson, S., Olah, M.E., Mallol, J., Canela, E.I., Zoli, M., Agnati, L.F., Ibanez, C.F., Lluis, C., Franco, R., Ferre, S., Fuxe, K., Casadó, V., Scott, R., Terasmaa, A., Hansson, A., Watson, S., Olah, M.E., Mallol, J., Canela, E.I., Zoli, M., Agnati, L.F., Ibáñez, C.F., Lluis, C., Franco, R., Ferré, S., Fuxe, K., Casado, V., Scott, R., Terasmaa, A., Hansson, A., Watson, S., Olah, M.E., Mallol, J., Canela, E.I., Zoli, M., Agnati, L.F., Ibanez, C.F., Lluis, C., Franco, R., Ferre, S., Fuxe, K., 2002. Coaggregation, cointernalization, and codesensitization of adenosine A2A receptors and dopamine D2 receptors. J. Biol. Chem. 277, 18091–18097. https://doi.org/10.1074/jbc.M107731200.

Hradsky, J., Mikhaylova, M., Karpova, A., Kreutz, M.R., Zuschratter, W., 2013. Super-resolution microscopy of the neuronal calcium-binding proteins Calneuron-1 and Caldendrin. Methods Mol. Biol. 963, 147–169. https://doi.org/10.1007/978-1-62703-230-8_10.

Huang, L., Wu, D.D., Zhang, L., Feng, L.Y., 2013. Modulation of A2a receptor antagonist on D2 receptor internalization and ERK phosphorylation. Acta Pharmacol. Sin. 34, 1292–1300. https://doi.org/10.1038/aps.2013.87.

Jenner, P., 2014. An overview of adenosine A2A receptor antagonists in Parkinson's disease. Int. Rev. Neurobiol. 119, 71–86. https://doi.org/10.1016/B978-0-12-801022-8.00003-9.

Jenner, P., Mori, A., Aradi, S.D., Hauser, R.A., 2021. Istradefylline – A First Generation Adenosine A2A Antagonist for the Treatment of Parkinson's Disease, 21, pp. 317–333. https://doi.org/10.1080/14737175.2021.1880896.

Lanciego, José L., Wouterlood, F.G., Erro, E., Giménez-Amaya, J.M., 1998a. Multiple axonal tracing: simultaneous detection of three tracers in the same section. Histochem. Cell Biol. 110, 509–515. https://doi.org/10.1007/s004180050312.

Lanciego, J.L., Luquin, M.R., Guillén, J., Giménez-Amaya, J.M., 1998b. Multiple neuroanatomical tracing in primates. Brain Res. Brain Res. Protoc. 2, 323–332. https://doi.org/10.1016/s1385-299x(98)00007-5.

Lanciego, J.L., Vázquez, A., 2012. The basal ganglia and thalamus of the long-tailed macaque in stereotaxic coordinates. A template atlas based on coronal, sagittal and horizontal brain sections. Brain Struct. Funct. 217, 613–666. https://doi.org/10.1007/s00429-011-0370-5.

Lopez-Lopez, A., Labandeira, C.M., Labandeira-Garcia, J.L., Muñoz, A., 2020. Rho kinase inhibitor fasudil reduces l-DOPA-induced dyskinesia in a rat model of Parkinson's disease. Br. J. Pharmacol. 177, 5622–5641. https://doi.org/10.1111/BPH.15275.

Mizuno, Y., Kondo, T., 2013. Adenosine A2A receptor antagonist istradefylline reduces daily OFF time in Parkinson's disease. Mov. Disord. 28, 1138–1141. https://doi.org/10.1002/mds.25418.

Morano, A., Jiménez-Jiménez, F.J., Molina, J.A., Antolín, M.A., 1994. Risk-factors for Parkinson's disease: case-control study in the province of Cáceres, Spain. Acta Neurol. Scand. 89, 164–170. https://doi.org/10.1111/j.1600-0404.1994.tb01655.x.

Morelli, M., Di Paolo, T., Wardas, J., Calon, F., Xiao, D., Schwarzschild, M.A., 2007. Role of adenosine A2A receptors in parkinsonian motor impairment and l-DOPA-induced motor complications. Prog. Neurobiol. 83, 293–309. https://doi.org/10.1016/j.pneurobio.2007.07.001.

Mori, A., 2020. How do adenosine A2A receptors regulate motor function? Parkinsonism Relat. Disord. 80 (Suppl. 1), S13–S20. https://doi.org/10.1016/J.PARKRELDIS.2020.09.025.

Muñoz, A., Garrido-Gil, P., Dominguez-Meijide, A., Labandeira-Garcia, J.L., 2014. Angiotensin type 1 receptor blockage reduces l-dopa-induced dyskinesia in the 6-OHDA model of Parkinson's disease. Involvement of vascular endothelial growth factor and interleukin-1ß. Exp. Neurol. 261, 720–732. https://doi.org/10.1016/j.expneurol.2014.08.019.

Navarro, G., Carriba, P., Gandía, J., Ciruela, F., Casadó, V., Cortés, A., Mallol, J., Canela, E.I., Lluis, C., Franco, R., 2008. Detection of heteromers formed by cannabinoid CB1, dopamine D2, and adenosine A2A G-protein-coupled receptors by combining bimolecular fluorescence complementation and bioluminescence energy transfer. Sci. World J. 8, 1088–1097. https://doi.org/10.1100/tsw.2008.136.

Navarro, G., Ferré, S., Cordomi, A., Moreno, E., Mallol, J., Casadó, V., Cortés, A., Hoffmann, H., Ortiz, J., Canela, E.I., Lluís, C., Pardo, L., Franco, R., Woods, A.S., 2010. Interactions between intracellular domains as key determinants of the quaternary structure and function of receptor heteromers. J. Biol. Chem. 285, 27346–27359. https://doi.org/10.1074/jbc.M110.115634.

Navarro, G., Cordomí, A., Brugarolas, M., Moreno, E., Aguinaga, D., Pérez-Benito, L., Ferre, S., Cortés, A., Casadó, V., Mallol, J., Canela, E.I., Lluís, C., Pardo, L., McCormick, P.J., Franco, R., 2018. Cross-communication between Gi and Gs in a G-protein-coupled receptor heterotetramer guided by a receptor C-terminal domain. BMC Biol. 16 (24), 1–15. https://doi.org/10.1186/s12915-018-0491-x.

Oñatibia-Astibia, A., Franco, R., Martínez-Pinilla, E., 2017. Health benefits of methylxanthines in neurodegenerative diseases. Mol. Nutr. Food Res. 61 https://doi.org/10.1002/mnfr.201600670, 1600670.

Orr, A.G., Hsiao, E.C., Wang, M.M., Ho, K., Kim, D.H., Wang, X., Guo, W., Kang, J., Yu, G.-Q., Adame, A., Devidze, N., Dubal, D.B., Masliah, E., Conklin, B.R., Mucke, L., 2015. Astrocytic adenosine receptor A2A and Gs-coupled signaling regulate memory. Nat. Neurosci. 18, 423–434. https://doi.org/10.1038/nn.3930.

Orru, M., Bakešová, J., Brugarolas, M., Quiroz, C., Beaumont, V., Goldberg, S.R., Lluís, C., Cortés, A., Franco, R., Casadó, V., Canela, E.I., Ferré, S., 2011. Striatal pre- and postsynaptic profile of adenosine A2A receptor antagonists. PLoS One 6, e16088. https://doi.org/10.1371/journal.pone.0016088.

Parent, A., Hazrati, L.N., 1993. Anatomical aspects of information processing in primate basal ganglia. Trends Neurosci. 16, 111–116. https://doi.org/10.1016/0166-2236(93)90135-9.

Perreault, M.L., Hasbi, A., Shen, M.Y.F., Fan, T., Navarro, G., Fletcher, P.J., Franco, R., Lanciego, J.L., George, S.R., 2016. Disruption of a dopamine receptor complex amplifies the actions of cocaine. Eur. Neuropsychopharmacol. 26, 1366–1377. https://doi.org/10.1016/j.euroneuro.2016.07.008.

Pinna, A., Bonaventura, J., Farré, D., Sánchez, M., Simola, N., Mallol, J., Lluís, C., Costa, G., Baqi, Y., Müller, C.E., Cortés, A., McCormick, P., Canela, E.I., Martínez-Pinilla, E., Lanciego, J.L., Casadó, V., Armentero, M.-T., Franco, R., 2014. L-DOPA disrupts adenosine a(2A)-cannabinoid CB(1)-dopamine D(2) receptor heteromer cross-talk in the striatum of hemiparkinsonian rats: biochemical and behavioral studies. Exp. Neurol. 253, 180–191. https://doi.org/10.1016/j.expneurol.2013.12.021.

Qi, H., Li, S., 2014. Dose-response meta-analysis on coffee, tea and caffeine consumption with risk of Parkinson's disease. Geriatr Gerontol Int 14, 430–439. https://doi.org/10.1111/ggi.12123.

Rajakumar, N., Elisevich, K., Flumerfelt, B.A., 1993. Biotinylated dextran: a versatile anterograde and retrograde neuronal tracer. Brain Res. 607, 47–53. https://doi.org/10.1016/0006-8993(93)91488-e.

Raykova, D., Kermpatsou, D., Malmqvist, T., Harrison, P.J., Sander, M.R., Stiller, C., Heldin, J., Leino, M., Ricardo, S., Klemm, A., David, L., Spjuth, O., Vemuri, K., Dimberg, A., Sundqvist, A., Norlin, M., Klaesson, A., Kampf, C., Söderberg, O., 2022.

A method for Boolean analysis of protein interactions at a molecular level. Nat. Commun. 13 https://doi.org/10.1038/S41467-022-32395-W.

Rosin, Diane L., Robeva, A., Woodard, R.L., Guyenet, P.G., Linden, J., 1998. Immunohistochemical localization of adenosine a(2A) receptors in the rat central nervous system. J. Comp. Neurol. 401, 163–186. https://doi.org/10.1002/(SICI)1096-9861(19981116)401:2<163::AID-CNE2>3.0.CO;2-D.

Ross, G.W., Petrovitch, H., 2001. Current evidence for neuroprotective effects of nicotine and caffeine against Parkinson??S disease. Drugs Aging 18, 797–806. https://doi.org/10.2165/00002512-200118110-00001.

Sahlholm, K., Gómez-Soler, M., Valle-León, M., López-Cano, M., Taura, J.J., Ciruela, F., Fernández-Dueñas, V., 2018. Antipsychotic-like efficacy of dopamine D2 receptor-biased ligands is dependent on adenosine A2A receptor expression. Mol. Neurobiol. 55, 4952–4958. https://doi.org/10.1007/S12035-017-0696-Y.

Saki, M., Yamada, K., Koshimura, E., Sasaki, K., Kanda, T., 2013. In vitro pharmacological profile of the A2A receptor antagonist istradefylline. Naunyn Schmiedeberg's Arch. Pharmacol. 386, 963–972. https://doi.org/10.1007/s00210-013-0897-5.

Sako, W., Murakami, N., Motohama, K., Izumi, Y., Kaji, R., 2017. The effect of istradefylline for Parkinson's disease: a meta-analysis. Sci. Rep. 71 (7), 1–7. https://doi.org/10.1038/s41598-017-18339-1.

Schwarzschild, M.A., Chen, J.-F., Ascherio, A., 2002. Caffeinated clues and the promise of adenosine a(2A) antagonists in PD. Neurology 58, 1154–1160. https://doi.org/10.1212/WNL.58.8.1154.

Schwarzschild, M.A., Agnati, L., Fuxe, K., Chen, J.-F., Morelli, M., 2006. Targeting adenosine A2A receptors in Parkinson's disease. Trends Neurosci. 29, 647–654. https://doi.org/10.1016/j.tins.2006.09.004.

Stojanovic, T., Orlova, M., Sialana, F.J., Höger, H., Stuchlik, S., Milenkovic, I., Aradska, J., Lubec, G., 2017. Validation of dopamine receptor DRD1 and DRD2 antibodies using receptor deficient mice. Amino Acids 49, 1101–1109. https://doi.org/10.1007/S00726-017-2408-3.

Strömberg, I., Popoli, P., Müller, C.E., Ferré, S., Fuxe, K., 2000. Electrophysiological and behavioural evidence for an antagonistic modulatory role of adenosine A2A receptors in dopamine D2 receptor regulation in the rat dopamine-denervated striatum. Eur. J. Neurosci. 12, 4033–4037. https://doi.org/10.1046/J.1460-9568.2000.00288.X.

Surmeier, D.J., Graves, S.M., Shen, W., 2014. Dopaminergic modulation of striatal networks in health and Parkinson's disease. Curr. Opin. Neurobiol. 29, 109–117. https://doi.org/10.1016/J.CONB.2014.07.008.

Tozzi, A., De Iure, A., Di Filippo, M., Tantucci, M., Costa, C., Borsini, F., Ghiglieri, V., Giampà, C., Fusco, F.R., Picconi, B., Calabresi, P., 2011. The distinct role of medium spiny neurons and cholinergic interneurons in the D_2/A_2A receptor interaction in the striatum: implications for Parkinson's disease. J. Neurosci. 31, 1850–1862. https://doi.org/10.1523/JNEUROSCI.4082-10.2011.

Trifilieff, P., Rives, M.L., Urizar, E., Piskorowski, R.A., Vishwasrao, H.D., Castrillon, J., Schmauss, C., Slättman, M., Gullberg, M., Javitch, J.A., 2011. Detection of antigen interactions ex vivo by proximity ligation assay: endogenous dopamine D2-adenosine A2A receptor complexes in the striatum. Biotechniques 51, 111–118. https://doi.org/10.2144/000113719.

Veenman, C.L., Reiner, A., Honig, M.G., 1992. Biotinylated dextran amine as an anterograde tracer for single- and double-labeling studies. J. Neurosci. Methods 41, 239–254. https://doi.org/10.1016/0165-0270(92)90089-v.

Verma, V., Hasbi, A., ODowd, B.F., George, S.R., O'Dowd, B.F., George, S.R., 2010. Dopamine D1-D2 receptor Heteromer-mediated calcium release is desensitized by D1 receptor occupancy with or without signal activation: dual functional regulation by G protein-coupled receptor kinase 2. J. Biol. Chem. 285, 35092–35103. https://doi.org/10.1074/jbc.M109.088625.

Woods, A.S., Ciruela, F., Fuxe, K., Agnati, L.F., Lluis, C., Franco, R., Ferré, S., 2005. Role of electrostatic interaction in receptor-receptor heteromerization. J. Mol. Neurosci. 26, 125–132. https://doi.org/10.1385/JMN:26:2-3:125.

Wouterlood, F.G., Jorritsma-Byham, B., 1993. The anterograde neuroanatomical tracer biotinylated dextran-amine: comparison with the tracer Phaseolus vulgaris-leucoagglutinin in preparations for electron microscopy. J. Neurosci. Methods 48, 75–87. https://doi.org/10.1016/S0165-0270(05)80009-3.